

LEARNING TO INTERACT IN WORLD LATENT FOR TEAM COORDINATION

Dongsu Lee¹ Daehee Lee² Yaru Niu³ Honguk Woo² Amy Zhang^{1†} Ding Zhao^{3†}
¹University of Texas at Austin ²Sungkyunkwan University ³Carnegie Mellon University
 dongsu.lee@utexas.edu † Equally Advising

ABSTRACT

This work presents a novel representation learning framework, *interactive world latent* (IWOL), to facilitate *team coordination* in multi-agent reinforcement learning (MARL). Building effective representation for team coordination is a challenging problem, due to the intricate dynamics emerging from multi-agent interaction and incomplete information induced by local observations. Our key insight is to construct a learnable representation space that jointly captures inter-agent relations and task-specific world information by directly modeling communication protocols. This representation, we maintain fully decentralized execution with implicit coordination, all while avoiding the inherent drawbacks of explicit message passing, *e.g.*, slower decision-making, vulnerability to malicious attackers, and sensitivity to bandwidth constraints. In practice, our representation can be used not only as an implicit latent for each agent, but also as an explicit message for communication. Across four challenging MARL benchmarks, we evaluate both variants and show that IWOL provides a simple yet powerful key for team coordination. Moreover, we demonstrate that our representation can be combined with existing MARL algorithms to further enhance their performance.

1 INTRODUCTION

Representation learning has become a foundational paradigm, leading to significant advances in computer vision (Roh et al., 2021), natural language processing (Liu et al., 2023), and, more recently, learning-based control (Hafner et al., 2025; Espeholt et al., 2018). Within imitation learning and reinforcement learning (RL), structured latent variables such as successor features (Sun et al., 2025; Agarwal et al., 2024), temporal distance embedding (Wang et al., 2023; Ma et al., 2023), skill embedding (Pertsch et al., 2021; Wang et al., 2024c), and symbolic representation (Landajuela et al., 2021; Christoffersen et al., 2023) have improved sample efficiency and policy generalization. By contrast, effective representation learning in MARL remains relatively underexplored. Furthermore, partial observability and complex credit assignment blur the learning signal, hindering agents from acquiring representations for team coordination in their shared environment (Guan et al., 2022).

This work studies how to build a representation for a multi-agent system with the following question:

What information should a latent representation for team coordination capture to enable coordinated control from partial and noisy local observations?

We argue that an effective representation for team coordination should capture at least two-fold: (i) inter-agent relations (Sukhbaatar et al., 2016; Foerster et al., 2016; Jiang & Lu, 2018), who influences whom, and how complementary their roles are, and (ii) task-specific world information, *i.e.*, a compact surrogate of the privileged global information (Cai et al., 2024; Li et al., 2024b; Ndousse et al., 2021; Salter et al., 2021). Such representation provides sufficient information for downstream control, permutation-invariant to agent ordering, and scalable with team size, so that decentralized policies can reason consistently about a shared environment despite non-stationarity and credit assignment challenges (Omidshafiei et al., 2017; Dibangoye & Buffet, 2018; Lee & Kwon, 2024a).

We address this question by learning an *interactive world representation* through an encoder, trained with two decoders that align such a representation with the factors needed for coordination. More precisely, *interactive* and *world* decoders reconstruct pairwise interaction signals between agents,

which are extracted by a graph-attention mechanism (Veličković et al., 2018), and privileged state features, respectively. Note that two decoders and a graph-attention module are used only at training time as guidance; at execution, each agent conditions on its local observation to produce a unified representation without any decoder or message exchange, yielding a fully decentralized (and thus implicit) use of the learned representation. While the graph-attention approach resembles a communication module (Niu et al., 2021; Hu et al., 2024b; Pina et al., 2024), in $IWOL$ it serves primarily as a representation learner; if desired, the same backbone can expose as explicit messages at test time.

Contribution: (i) Firstly, this work proposes a novel representation learning framework for multi-agent coordination, *interactive world latent* ($IWOL$) that encodes both inter-agent relations and privileged world information at a task level. (ii) Secondly, $IWOL$ extends the line of communication MARL by introducing a communication scheduler based on graph-attention, which serves purely as a representation learner under an implicit communication scenario. In addition, this architecture naturally admits two variants: an *implicit* mode, where no messages are required at test time, and an *explicit* mode, where the learned messages are fed into the policy network for message-rich coordination. (iii) Lastly, to demonstrate the efficiency of $IWOL$, we compare the proposed solution with MARL baselines across four challenging multiple robotics testbeds, *including* autonomous driving (Li et al., 2022b), swarm-robot coordination (Pickem et al., 2017), bimanual dexterous hand manipulation (Chen et al., 2022), and multiple quadruped robots coordination (Xiong et al., 2024).

2 RELATED WORKS

Cooperative Multi-agent Reinforcement Learning. Transcending the single-agent environment, MARL has received attention to tackle robotics and other domains of the real world; the fact that each agent relies on a noisy and local observation of the environment further compounds coordination difficulties (Yang et al., 2023; He et al., 2022). To surmount these challenges and foster cooperative behavior, several approaches have been proposed that enable agents to learn effective strategies through the joint optimization of a shared team objective in online settings. The centralized training and decentralized execution (CTDE) framework is widely used as a promising alternative (Zhang et al., 2021). This framework leverages global state information during training to alleviate partial observability while each agent learns a decentralized policy that relies solely on local observations during execution (Yu et al., 2022a; Lowe et al., 2017; Qu et al., 2020; Rashid et al., 2020; Dou et al., 2022; Li et al., 2022a; Foerster et al., 2018; Li et al., 2021a; Shao et al., 2023; Wen et al., 2022; Zhu et al., 2024). This work introduces a novel MARL algorithm that models the interactive world latent using a communication protocol, enabling robust performance in cooperative MARL tasks.

Communication for Multi-agent Coordination. Inter-agent communication is a linchpin to facilitate effective multi-agent coordination in MARL, fostering synergistic collaboration between agents. Most seminal works in MARL have centered on explicit communication protocols, where agents exchange messages to gain a clear understanding of others’ context; for example, predefined full communication (Foerster et al., 2016; Sukhbaatar et al., 2016), partial communication (Wang et al., 2020; Yuan et al., 2022), learnable communication with adaptive gating mechanisms (Jiang & Lu, 2018; Singh et al., 2019; Ding et al., 2020; Hu et al., 2024b). These solutions frequently impose heavy communication burdens, making them unsuitable for real-world scenarios with limited bandwidth while also being vulnerable to adversarial attacks (Dafoe et al., 2020; Grimbly et al., 2021; Yuan et al., 2023). To address these challenges, we propose a communication protocol that learns inter-agent relations as an interactive latent. This design embeds coordination cues directly into the latent, enabling message-free deployment and decentralized, efficient inference.

Representation for Multi-agent Reinforcement Learning. Representation is critical for RL improvement, empowering agents to distill complex observations into useful abstractions that drive more informed decision-making. In MARL, individual agents use representation not only to better encode their local observations but also to facilitate the encoding of intricate inter-agent interactions or underlying world dynamics. Several works build representation in MARL, such as information reconstruction (Kim et al., 2023; Kang et al., 2025), auxiliary task-specific predictions (Shang et al., 2021), marginal utility function (Gu et al., 2022), self-predictive learning (Huh & Mohapatra, 2024; Feng et al., 2023), contrastive learning (Hu et al., 2024c; Song et al., 2023), and communication protocol (Jiang & Lu, 2018; Niu et al., 2021; Hu et al., 2024b). While these studies have advanced MARL representation learning, they focus narrowly on specific aspects, *e.g.*, local observation embedding, inter-agent relationships, or world dynamics, without integrating them. Such approaches

can lead to fragmented representations that may hinder agents from forming an understanding of their environment. This work proposes the IWOL framework that leverages privileged information during the training communication module to capture inter-agent relationships and world information.

3 BACKGROUNDS AND PROBLEM FORMULATION

Decentralized Partially Observable MDP. We formulate the MARL problem using a decentralized partially observable Markov decision process (Dec-POMDP) (Bernstein et al., 2002) \mathcal{M} , which is formally characterized by the tuple $\langle \mathcal{I}, \mathcal{S}, \mathcal{O}_i, \mathcal{A}_i, \mathcal{T}, \Omega_i, r_i, \gamma \rangle$, where $\mathcal{I} = 1, 2, \dots, I$ denotes a set of agents. Here, \mathcal{S} represents the global state space; \mathcal{O}_i and \mathcal{A}_i correspond to the observation and action spaces specific to agent i , respectively. The state transition dynamics are captured by $\mathcal{T} : \mathcal{S} \times \mathcal{A}_1 \times \dots \times \mathcal{A}_I \mapsto \mathcal{S}$, while $\Omega_i : \mathcal{S} \mapsto \mathcal{O}_i$ specifies the observation function for agent i . Each agent i receives rewards according to its reward function $r_i : \mathcal{S} \times \mathcal{A}_1 \times \dots \times \mathcal{A}_I \mapsto \mathbb{R}$, and aims to maximize its discounted cumulative reward given by $R_i^t = \sum_{k=t}^{T-1} \gamma^{k-t} r_i^k$, with the temporal discount factor $\gamma \in [0, 1)$. Consistent with previous literature in communication-based reinforcement learning, we assume a deterministic MDP throughout this work, unless explicitly stated otherwise.

Problem Setup. We posit each agent i has access only to its own local observation o_i^t and must act without direct knowledge of the global state. Under such partial observability and interdependence, successful team performance hinges on effective coordination via synchronous communication. Concretely, we introduce a learnable protocol $P : M_1^0 \times \dots \times M_I^0 \mapsto M_1 \times \dots \times M_I$ that transforms each agent’s raw message $m_i^{t,0} \in M_i^0$ into a processed message $m_i^t \in M_i$. At every timestep t , all agents emit $m_i^{t,0}$, receive their corresponding m_i^t from P , and then select actions.

Within the CTDE framework, our objective is to jointly learn the policies $\{\pi_i\}_{i \in \mathcal{I}}$ and the communication protocol P so as to maximize the team’s cumulative discounted return. To achieve it, we consider both implicit and explicit communication protocols.

On-policy Optimization. Our proposed solution is based on the on-policy optimization method, the multi-agent proximal policy optimization (MAPPO) algorithm (Schulman et al., 2017; Yu et al., 2022a). Based on this, we train all modules of a framework in an end-to-end manner under online settings. The loss for policy and value function is defined as follows:

$$\mathcal{L}_\pi(\phi_i) = -\min(p_i^t A_i^t, \text{clip}(p_i^t, 1 - \epsilon, 1 + \epsilon) A_i^t) - \mathcal{H}(\pi_{\phi_i}(a_i^t | o_i^t)), \quad (1)$$

where ϕ_i is parameter of agent i -th actor network, $p_i^t = \frac{\pi_{\phi_i}(a_i^t | o_i^t)}{\pi_{\theta^{\text{old}}}(a_i^t | o_i^t)}$ is the probability ratio, A_i^t is an advantage estimate, and ϵ is a clipping parameter typically set to a small value. The additional entropy term $\mathcal{H}(\pi_{\phi_i}(a_i^t | o_i^t))$ encourages exploration by penalizing overly confident policies.

Next, the centralized critic parameters θ are updated via a clipped value loss to stabilize learning with the shared observation $\mathbf{o}^t = [o_1^t, \dots, o_I^t]$ or state s^t , as follows:

$$\mathcal{L}_V(\theta) = \max\left(\ell_\delta(R^t - V_\theta(\mathbf{o}^t)), \ell_\delta(R^t - V_\theta^{\text{clip}}(\mathbf{o}^t))\right), \quad (2)$$

$$\text{where } V_\theta^{\text{clip}}(\mathbf{o}^t) = V_{\theta^{\text{old}}}(\mathbf{o}^t) + \text{clamp}(V_{\theta_i}(\mathbf{o}^t) - V_{\theta^{\text{old}}}(\mathbf{o}^t), -\epsilon, \epsilon)$$

and $\ell_\delta(\cdot)$ is the Huber loss (Huber, 1992), which is less sensitive to outliers than a standard MSE loss.

4 INTERACTIVE WORLD LATENT (IWOL)

In this section, we first show a motivating example of when explicit communication fails in 4.1, introduce IWOL in Section 4.2, and then explain how to train it in Section 4.3.

4.1 A MOTIVATING EXAMPLE

Figure 1 shows performance degradation in a simple traffic junction (Sukhbaatar et al., 2016) where multiple agents rely on explicit message passing to coordinate their movements. While unconstrained communication achieves nearly perfect success (Normal), imposing a bandwidth limit (Li & Zhang, 2024) reduces performance by about 10 ~ 30% (Type I), and a message-corruption attack (Sun et al., 2023) leads

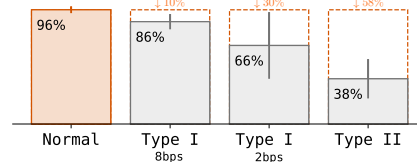


Figure 1: **A motivating example.** Explicit communication’s performance degradation in two challenging scenarios: Type I. Bandwidth (bits per second) constraint; Type II. Communication attack.

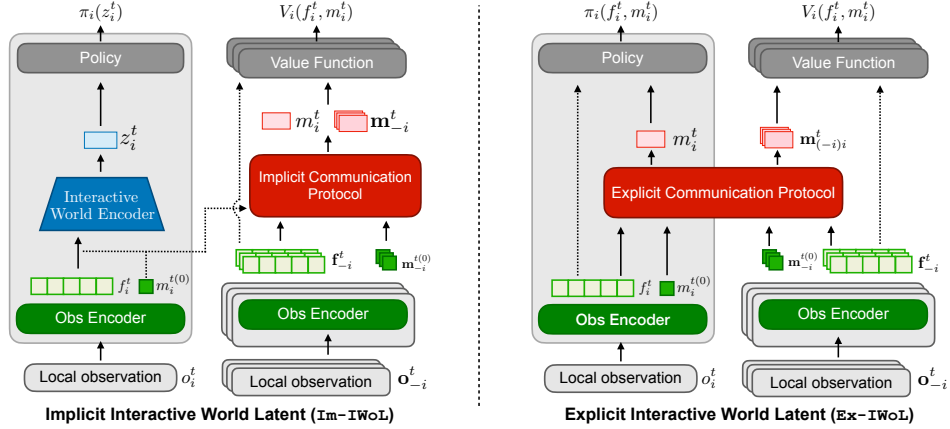


Figure 2: **Overview diagram of IWOL framework.** Grey box represents each agent. (Left) Implicit variation of IWOL. In this variation, each agent does not use communication messages at execution time. (Right) Explicit variation of IWOL. Policy directly uses a communication message from an explicit communication protocol. Note that IWOL’s value function is decentralized, and it uses its own message and local embedding $V_{\theta_i}(m_i^t, f_i^t)$. Herein, \cdot_{-i} means all agent’s elements except i , and $\cdot_{(-i)i}$ includes all agent’s elements including i .

to a severe performance drop (Type II), *i.e.*, approximately 60%. This dramatic degradation under realistic constraints and adversarial conditions reveals the fragility of explicit channels. To ensure robust multi-agent coordination, we thus advocate for the necessity of *implicit communication* in which message changes only happen within training. That is because the implicit communication method naturally overcomes these issues. Please see the Appendix D for details of this toy example.

4.2 INTERACTIVE WORLD LATENT FOR MULTI-AGENT COORDINATION

Our desiderata are twofold: first, to avoid explicit message passing, but maintain team coordination under multi-agent dynamics and partial observability; and second, to maintain simplicity by refraining from additional modules, thereby enabling faster decision-making. Therefore, we learn a latent representation from local observations, encoding inter-agent relations and task-specific world information. To this end, we redesign the communication protocol to serve our representation learning objective.

Architectural Design. Figure 2 shows an overview for IWOL. First, each agent i employs an observation encoder depicted in Figure 3 to transform its raw local observation o_i^t into other modules. Specifically, o_i^t is processed by a self-attention, which produces an intermediate embedding f_i^t . This embedding is then forwarded through an MLP, which outputs the initial message $m_i^{t(0)} \in \mathbb{R}^d$, denoted as round 0. It serves as the raw input to the subsequent communication protocol. Formally, we may write

$$[f_i^t, m_i^{t(0)}] = \text{Encoder}(\text{Attn}(o_i^t))$$

where Attn denotes the self-attention and Encoder denotes the MLP.

Next, the communication protocol block, visualized in Figure 4, is implemented with attention mechanisms to adaptively select neighbors and refine their messages in one go. Especially, each agent’s feature f_i^t is fed into an additive-attention and GumbelSoftmax block to produce a discrete adjacency mask. This mask is a relationship graph that guides a Transformer block that performs L rounds of attention-based message aggregation and refinement, mapping the initial message $m_i^{t(0)}$ directly to the final message m_i^t . This design allows the communication block to serve directly as a protocol for inter-agent coordination.

Lastly, the previously produced vectors, *e.g.*, communication message m_i^t and intermediate embedding f_i^t , are used as input to policy and value function networks. We design a policy network ϕ_i and the value function network θ_i as a feed-forward layer. Herein, a policy network is set in a stochastic form.

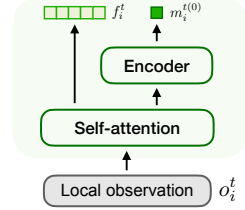


Figure 3: **Design for observation encoder.**

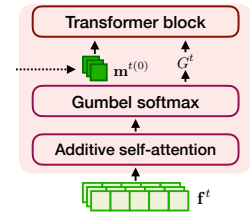


Figure 4: **Design for communication protocol.**

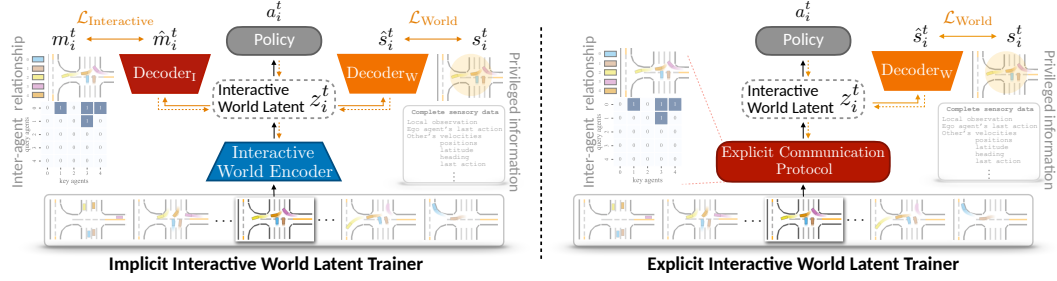


Figure 5: **Diagram for Interactive World Latent Modeling.** Solid and dotted lines denote forward and backward processes. The orange line implies only work in training. (Left) Im-IWOL uses the world and interactive decoder to reconstruct the privileged state and communication message $\hat{m}_i^t = \text{Decoder}_I(z_i^t)$. (Right) Ex-IWOL sets the latent to the message vector $z_i^t = m_i^t$, and then uses the world decoder to reconstruct the privileged state $\hat{s}_i^t = \text{Decoder}_W(z_i^t)$, thereby encouraging z_i^t to embed the global information s_i^t .

Graph-attention Communication Protocol. Our communication protocol first generates a topology graph that captures the relationship between agents as follows: $\{g_{ij}^t\}_{i,j=1}^I = \text{GumbelSoftmax}(\text{AddAtt}(\{f_k^t\}_{k=1}^I))$ where $\text{AddAtt}(\cdot) = (a_{gg})^\top [W_{gg}f_i \| W_{gg}f_j]$, where AddAtt is additive attention, a_{gg} is attention coefficient, and W_{gg} is a learned weight matrix. To build a topology graph G^t , we hierarchically use a proximity mask to reflect a physical communication range. This mask is activated when $\|\mathbf{x}_i^t - \mathbf{x}_j^t\| \leq d_{\text{comm}}$, where \mathbf{x}_i and d_{comm} denotes the position of agent i and a minimum distance for communication. Next, a Transformer block then propagates messages over G^t , yielding per-agent initial message $m_i^{t(0)}$. Final message vector m_i^t can be interpreted as an *interactive latent* that encodes the relationship among agents.

Interactive World Latent Modeling. Figure 5 visualizes an overview diagram about how to model IWOL explicitly and implicitly. Our goal is to build an interactive world latent z_i^t that captures inter-agent relationships and privileged world information for efficient multi-agent coordination. For this, the implicit IWOL (Im-IWOL) variant includes the following three modules.

$$\underbrace{z_i^t = \text{Encoder}_{\text{IW}}(f_i^t)}_{\text{Interactive World Encoder}} \quad \underbrace{\hat{m}_i^t = \text{Decoder}_I(z_i^t)}_{\text{Interactive Decoder}} \quad \underbrace{\hat{s}_i^t = \text{Decoder}_W(z_i^t)}_{\text{World Decoder}}$$

The world decoder reconstructs the agent’s privileged state s_i^t , encouraging z_i^t to embed task-specific global signals beyond local observation, whereas the interactive decoder reconstructs communication messages m_i^t , forcing z_i^t to preserve inter-agent dependencies.

For the implementation of the explicit IWOL (Ex-IWOL), we eliminate the interactive world encoder $\text{Encoder}_{\text{IW}}$ and instead reuse the explicit message emitted by the communication module itself, $z_i^t = m_i^t$, so we only use the world decoder Decoder_W for training. While this design simplifies the latent construction and leverages explicit communication, Im-IWOL instead learns a representation from raw observations, which can easily capture more integrated interaction and world features.

Remark: Compatibility of IWOL ’s latent representation with two communication variants

In basic, IWOL is implemented as an *implicit* mode that only routes m_i^t to the value network, not the policy network. *Explicit* communication mode routes m_i^t to policy and value networks. The policy has direct access to relational signals between agents in the execution phase, while the value network uses the same structure to assign more accurate credit during training.

4.3 TRAINING

Objective Function for Policy Training of IWOL . To extract a policy, both variants of IWOL can be optimized in an end-to-end manner with a composite objective function as follows:

$$\underbrace{\mathcal{L}_\pi^{\text{Im}}(\phi_i) = \mathcal{L}_\pi^{\text{RL}}(\phi_i) + \lambda_W \mathcal{L}_W + \lambda_I \mathcal{L}_I}_{\text{Implicit Variants Objective}} \quad \text{and} \quad \underbrace{\mathcal{L}_\pi^{\text{Ex}}(\phi_i) = \mathcal{L}_\pi^{\text{RL}}(\phi_i) + \lambda_W \mathcal{L}_W}_{\text{Explicit Variants Objective}}, \quad (3)$$

where individual terms reflect distinct training signals.

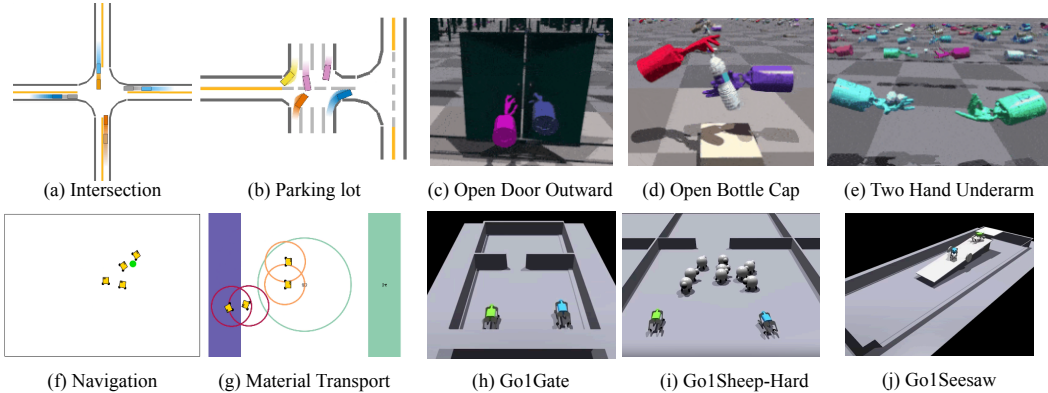


Figure 6: **Visualization of the experimental scenarios where we evaluate IWOL.** The top row contains MetaDrive (a-b) and Bi-DexHands environments (c-e), and the bottom row includes Robotarium (f-g) and multiagent-quadruped-environments (h-j).

RL policy objective $\mathcal{L}_{\pi}^{\text{RL}}(\phi_i)$ simply follows equation 1. World reconstruction objective \mathcal{L}_{W} encourages latent z_i^t (or m_i^t in the explicit variant) to capture the privileged state s_i^t that is only available during training; and communication message reconstruction objective \mathcal{L}_{I} asks the interactive decoder to reproduce the original communication message.

$$\mathcal{L}_{\text{W}} = \|\text{Decoder}_{\text{W}}(z_i^t) - s_i^t\|_2^2 \quad \text{and} \quad \mathcal{L}_{\text{I}} = \|\text{Decoder}_{\text{I}}(z_i^t) - m_i^t\|_2^2$$

The coefficients λ_s and λ_m balance auxiliary supervision against the RL signal, then we set $\lambda_s > 0$ in both modes but choose $\lambda_m = 0$ for the explicit variant. We provide a pseudocode for the training algorithm and training details in the Appendix C.

5 EXPERIMENTS

In the following subsection, we introduce a suite of experiments designed to rigorously validate the efficacy of IWOL as a MARL framework. Specifically, our experiments will employ four multi-agent robotic tasks, selected to elucidate the five research questions. For our experiments, although we use shared or privileged information in training across all algorithms, this experimental setup is not fully observable since the input of the policy is directly limited. Please see the Appendix E and F for the experimental setup, detailed description of tasks, and additional empirical results, *including* ablations.

5.1 ENVIRONMENTAL SETUPS

We evaluate the proposed solution, EX-IWOL and IM-IWOL , across four MARL environments: MetaDrive (Li et al., 2022b), Robotarium (Pickem et al., 2017), Bi-DexHands (Chen et al., 2022), and multiagent-quadruped-environments (MQE) (Xiong et al., 2024), visualized in Figure 6.

MetaDrive is a lightweight, large-scale simulator that features realistic traffic scenarios such as intersections and parking lots where multiple autonomous vehicles must coordinate to avoid collisions and reach their destinations. Since all ego agents have limited observability, this environment provides a strong benchmark for testing how well MARL methods enable communication for multi-agent coordination in dense traffic systems. We train each model under 1M timesteps.

Robotarium is a remotely accessible multi-robot testbed, used to evaluate physical coordination in real-world swarm robotics settings. We consider two tasks: simple navigation and material transport, each requiring multiple robots to share local information and synchronize movement to avoid obstacles and reach common goals. Specifically, this environment tests cooperation and coordination ability through only inter-agent communication since ego agents do not use local perception devices (*e.g.*, camera or LiDAR). We set 0.5M training timesteps.

MQE is based on Isaac Gym (Makoviychuk et al., 2021) that supports multi-agent tasks for quadrupedal robots. It includes cooperative tasks (*e.g.*, Narrow Gate, Seesaw, and Shepherding Sheep) where Unitree Go1 robots must coordinate to manipulate objects or navigate shared terrain. Agents operate under a hierarchical policy framework where high-level commands are issued over

Table 1: **Performance evaluation.** We present a performance comparison across 10 tasks with four environments. These results are averaged over 4 seeds, and we report the two standard deviations after the \pm sign. We highlight the best performance in **bold** and the second best in underlined. Note that if no I is specified, $I = 2$. Basically, all tasks within the same testbed are ordered according to difficulty.

Scenarios	Metrics	MARL Baselines				Proposed		
		MAPPO	MAT	MAGIC	CommFormer	Ex-IWoL	Im-IWoL	
Metadrive	Intersection ($I = 8$)	Rewards	454.8 \pm 70.2	500.3 \pm 279.4	518.3 \pm 77.4	399.0 \pm 21.6	660.3 \pm 33.2	<u>650.1</u> \pm 35.8
		Success (%)	<u>97.7</u> \pm 2.3	84.2 \pm 29.5	96.3 \pm 2.3	12.4 \pm 10.3	98.3 \pm 3.8	97.1 \pm 3.0
		Safety (%)	94.8 \pm 5.2	76.0 \pm 35.4	99.1 \pm 0.9	9.6 \pm 4.8	<u>98.3</u> \pm 3.8	97.1 \pm 3.0
	Parking lot ($I = 5$)	Rewards	327.4 \pm 211.7	605.8 \pm 163.4	371.2 \pm 14.3	527.6 \pm 195.6	<u>619.7</u> \pm 79.6	808.6 \pm 51.0
		Success (%)	30.3 \pm 15.9	<u>55.3</u> \pm 15.3	26.2 \pm 3.7	43.9 \pm 12.5	54.1 \pm 8.8	63.7 \pm 9.8
		Safety (%)	33.8 \pm 11.3	<u>54.8</u> \pm 15.0	29.8 \pm 2.2	40.0 \pm 14.6	53.7 \pm 8.8	63.6 \pm 9.8
Average rewards		391.1	553.1	444.8	463.3	<u>640.0</u>	729.4	
Robotarium	Navigation ($I = 4$)	Rewards	-4.1 \pm 0.3	-4.2 \pm 0.3	-4.2 \pm 0.4	-4.0 \pm 0.2	-3.7 \pm 0.9	-3.5 \pm 0.4
		Safety (%)	100.0 \pm 0.0	100.0 \pm 0.0	100.0 \pm 0.0	100.0 \pm 0.0	100.0 \pm 0.0	100.0 \pm 0.0
	Material transport ($I = 4$)	Rewards	2.7 \pm 0.8	3.11 \pm 1.2	2.6 \pm 0.2	1.2 \pm 2.2	<u>3.6</u> \pm 0.1	3.8 \pm 0.1
		Safety (%)	96.1 \pm 3.9	100.0 \pm 0.0	99.5 \pm 0.05	100.0 \pm 0.00	100.0 \pm 0.0	100.0 \pm 0.0
		Left materials	18.3 \pm 7.9	12.4 \pm 10.8	28.6 \pm 18.4	27.4 \pm 11.0	4.7 \pm 6.0	<u>5.0</u> \pm 5.0
	Average rewards		-0.7	-0.5	-0.8	-1.4	<u>-0.05</u>	0.15
Multi Quadrapeds	Go1Gate	Rewards	191.6 \pm 385.2	270.8 \pm 544.5	610.6 \pm 815.7	-5.4 \pm 7.9	1570.2 \pm 247.8	1390.4 \pm 244.6
		Success (%)	21.7 \pm 34.9	23.5 \pm 43.0	57.2 \pm 49.9	0.4 \pm 0.8	99.3 \pm 1.4	<u>96.4</u> \pm 3.6
	Go1Sheep Hard	Rewards	1357.5 \pm 141.0	2834.9 \pm 1552.8	1284.9 \pm 10.2	1233.2 \pm 55.1	<u>3340.9</u> \pm 506.3	6043.1 \pm 76.9
		Success (%)	0.0 \pm 0.0	16.8 \pm 0.0	0.0 \pm 0.0	0.0 \pm 0.0	<u>23.1</u> \pm 13.5	48.2 \pm 2.4
	Go1Seesaw	Rewards	4.3 \pm 13.2	56.0 \pm 24.2	79.7 \pm 52.7	-37.6 \pm 5.1	<u>84.1</u> \pm 51.0	114.1 \pm 41.4
		Success (%)	0.0 \pm 0.0	1.7 \pm 2.8	3.6 \pm 7.0	0.0 \pm 0.0	<u>6.8</u> \pm 5.9	15.3 \pm 7.8
Average rewards		517.8	1053.9	658.4	437.3	<u>1665.1</u>	2515.9	
Bi-DexHands	Door Open Outward	Rewards	606.0 \pm 23.3	18.8 \pm 27.2	617.2 \pm 14.7	447.6 \pm 76.8	<u>620.1</u> \pm 3.8	623.5 \pm 7.5
		Success (%)	57.5 \pm 42.7	15.0 \pm 17.3	85.0 \pm 8.2	65.0 \pm 20.8	<u>92.5</u> \pm 5.0	95.0 \pm 5.8
	Open Bottle Cap	Rewards	385.8 \pm 48.8	164.6 \pm 61.9	383.1 \pm 111.7	401.7 \pm 103.1	<u>471.9</u> \pm 62.7	502.9 \pm 47.8
		Success (%)	17.5 \pm 20.6	7.5 \pm 9.6	42.5 \pm 20.6	50.0 \pm 12.9	<u>62.5</u> \pm 17.1	70.0 \pm 11.5
	Two Catch Underarm	Rewards	2.4 \pm 1.0	9.7 \pm 5.2	19.6 \pm 4.7	16.3 \pm 10.1	31.6 \pm 3.0	33.9 \pm 5.1
		Success (%)	0.0 \pm 0.0	0.0 \pm 0.0	5.0 \pm 5.8	2.5 \pm 5.0	<u>12.5</u> \pm 5.0	20.0 \pm 12.9
Average rewards		331.4	64.4	340.0	285.5	<u>374.5</u>	386.8	

pre-trained low-level locomotion policies, allowing researchers to isolate the effect of coordinated planning and locomotion. For this task, evaluation is performed based on goal completion and auxiliary criteria such as safety and efficiency. We set 10M training timesteps.

Bi-DexHands is a heterogeneous robotic manipulation and cooperation simulation built on Isaac Gym. Specifically, it is a multi-agent dexterous manipulation testbed, featuring two robotic Shadow Hands, each with 24 degrees of freedom (DoF), enabling precise bimanual coordination. Tasks, two catch underarms, open door outward, and open bottle cap, require communication and contact-rich interactions between the two hands. We set the training period as 10M, and its success rate is measured by a 10% unit (*i.e.*, 0%, 10%, \dots , 90%, 100%).

Baselines. To comprehensively evaluate the performance of IWOL, we benchmark it against four established on-policy MARL algorithms. For on-policy, model-free methods, we include **MAPPO** (Yu et al., 2022a), which employs a centralized critic to address non-stationarity by leveraging global state information during training, while utilizing decentralized actors for execution. Furthermore, we consider **MAT** (Wen et al., 2022), which frames MARL as a sequence modeling problem, employing Transformer networks for both actors and critics. For communication-based MARL approaches, we assess **MAGIC** (Niu et al., 2021), which integrates a scheduler composed of a graph-attention encoder and a differentiable hard attention mechanism to dynamically determine communication timing and targets, alongside a message processor utilizing GATs (Veličković et al., 2018) to handle inter-agent messages efficiently. Furthermore, we evaluate the **CommFormer** (Hu et al., 2024b), which conceptualizes the inter-agent communication architecture as a learnable graph, enabling adaptive and efficient information exchange among agents.

In our experiments, we employ four random seeds and represent 95% confidence intervals with shaded regions in figures or standard deviations in tables, unless otherwise stated. All evaluations are performed under decentralized, partially observable, and goal-conditioned conditions, offering a comprehensive benchmark to evaluate how well the MARL algorithm enables scalable and adaptive coordination in diverse scenarios with different physical and strategic complexities.

5.2 EXPERIMENTAL RESULTS AND RESEARCH Q&A

RQ1. How good is IWOL for MARL, compared to previous methods?

A: IWOL variations achieve the **best** or **second-best** performance and success rate on most tasks.

Table 1 summarizes the aggregated experimental results for the 10 MARL benchmarks. We find that IWOL empirically outperforms prior MARL baselines. Im-IWOL achieves the top score in 7 out of 10 tasks, with Ex-IWOL taking second in those; conversely, Ex-IWOL tops the remaining 3 tasks, with Im-IWOL finishing second, that is, together the two IWOL variants occupy the winner and runner-up in every task. On average, Im-IWOL outperforms the strongest baseline by +176.3 points on MetaDrive and improves the Robotarium average reward from -0.5 to $+0.15$. In particular, our approach achieves up to 48.2% and 20.0% in MQE and Bi-DexHands, where previous baselines record near-zero success in three tasks (Go1Sheep, Go1Seesaw, and Two Catch Underarm). These results demonstrate that IWOL not only excels in standard MARL benchmarks but also effectively handles robotic manipulation tasks where existing MARL baselines fail.

RQ2. Can IWOL maintain coordination performance under incomplete observations?

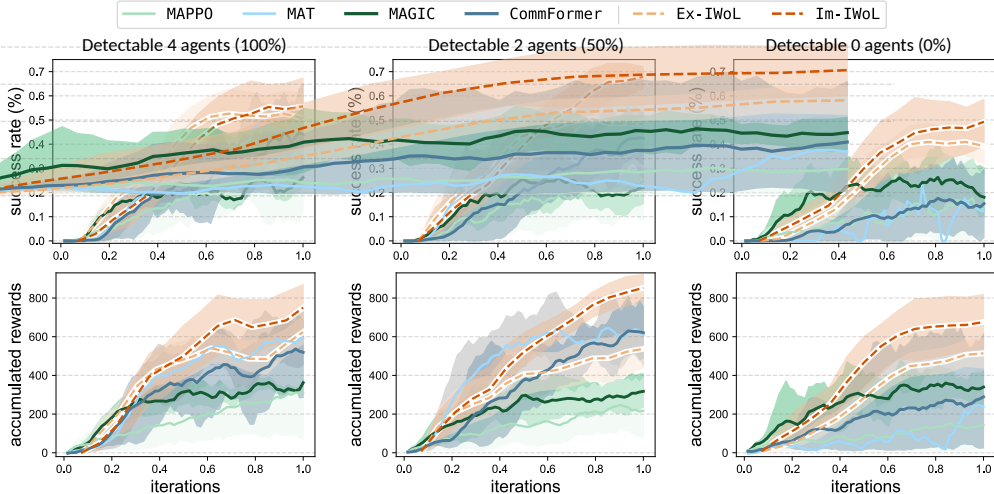


Figure 7: **Performance according to level of incomplete observations.** This presents the success rate and accumulated rewards as the number of detectable agents for the ego agent decreases in Parking Lot. This learning curve is plotted with the running average technique to differentiate baselines through a smoother line.

A: IWOL framework shows higher robustness than other baselines under incomplete observation scenarios.

In Figure 7, we present the success rate and accumulated reward as the number of detectable agents decreases. Such an experimental setup, as a communication-starved setting, is appropriate to study how well the proposed solution ensures robustness compared to baselines. This result demonstrates that both variants of IWOL maintain a clear margin over all baselines without severe drops in performance. Surprisingly, Im-IWOL always achieves above or about 50% of success rate and small drops with 0 detectable agents, whereas CommFormer and MAT lose roughly twice as much. Additionally, Ex-IWOL leverages explicit message encoding, yielding slightly faster gains, whereas Im-IWOL 's implicit latent construction delivers superior asymptotic performance.

RQ3. How effective is the world representation for the proposed and baseline solutions?

A: World representation yields a noticeable performance gain for communication MARL solutions, and the Transformer-based communication module is competitive with other baselines on itself.

Figure 8 shows the ablation results of the world representation across communication-based MARL algorithms, that is, whether Decoder_W is used during training. First, comparing IWOL variants with other baselines, we can see that it is competitive even without world representation embedding. This result implies that our Transformer-based communication protocol is powerful compared to other explicit communication baselines. Next, juxtaposing w/Decoder_W and w/oDecoder_W , we confirm that **variants** achieve better performances in most tasks and algorithms. Such empirical results directly demonstrate how effective and beneficial the world representation is for MARL training. Note that IWOL without its communication protocol and world latent is MAPPO.

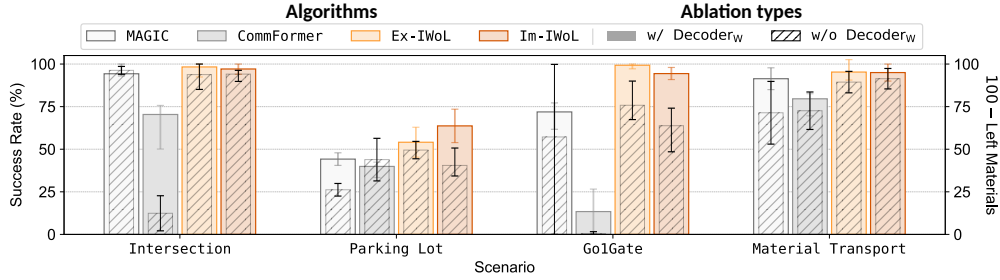


Figure 8: **Ablation study for world representation with Decoder_w**. The colored and dashed boxes indicate when `[there is no]` Decoder_w for world representation and when `[there is]`, respectively; that is, the `[colored]` performance is original for MAGIC and CommFormer, and the `[dashed]` performance is original for IWoL. For the Material Transport task, we use inverted metrics (right y -axis) for readability.

RQ4. Can IWoL maintain its performance as well in a large multi-agent system?

Table 2: **Scalability test**. We provide a success rate according to the number of agents in Intersection.

Algorithm	Success rate according to # of agents					# of agents	Baselines	
	4	8	16	32	48		MAPP0	MAGIC
Im-IWoL	99.5%±0.5	97.1%±3.0	95.2%±9.8	92.8%±16.5	86.6%±19.7	$ I = 4$	98.5±3.5	99.5±0.5
Ex-IWoL	99.1%±1.0	98.3%±3.8	98.0%±11.2	95.5%±19.0	91.0%±28.1	$ I = 48$	33.5±36.5	75.0±30.4

A: IWoL can maintain coordination performance decently as the agent population increases.

Table 2 reveals that coordination remains with good success rate with four agents, 99.5% for Im-IWoL, 99.1% for Ex-IWoL, and only marginally degrades as the team size doubles repeatedly, success stays above 95% up to 16 agents and above 92% (Im) / 95% (Ex) even at 32 agents. Remarkably, with 48 agents, Ex-IWoL still solves 91.0% of instances and Im-IWoL maintains 86.6%. In contrast, baselines suffer from a substantial performance drop from 4 to 48 agents. These observations confirm that IWoL has the potential to be adopted in large-scale MARL.

RQ5. Is Im-IWoL superior to the previous implicit communication branches?

Table 3: **Performance comparison with ICP**. We evaluate the performance of ICP across three variants.

Scenarios	Metrics	ICP-Dec	ICP-Sum	ICP-Monotonic	Im-IWoL
Parking Lot	Rewards	227.5±30.6	289.5±116.7	391.6±236.2	808.6±51.0
	Succ. Rate (%)	15.7±5.3	20.6±8.4	35.6±18.0	63.7±9.8
Go!Gate	Rewards	130.7±91.0	783.3±495.1	710.9±538.2	1390.4±244.6
	Succ. Rate (%)	5.8±6.6	70.5±15.5	67.8±22.0	96.4±3.6
Door Open Outward	Rewards	178.2±30.1	495.5±25.8	518.6±31.0	623.5±7.5
	Succ. Rate (%)	7.5±9.6	52.5±12.6	45.0±14.1	95.0±5.8

A: Although such a claim is not our focus, Im-IWoL outperforms the previous implicit method.

Table 3 demonstrates that our solution yields substantially higher rewards and success rates across all scenarios. Herein, ICP (Wang et al., 2025) works like inverse modeling, agents use predefined ‘scouting’ actions to encode messages and recover them by inverse mapping under ideal broadcast and decoding assumptions. In contrast, Im-IWoL learns the interactive world representation using a communication module during training, fusing privileged state and inter-agent relations. At deployment, Im-IWoL does not need additional modules, *e.g.*, communication or inference model.

Lastly, we would like to clarify that Im-IWoL is fundamentally different from previous branches; in other words, this claim is not our focus and core in this work. See the Appendix B and F for an extended literature survey of previous branches and experimental details.

6 CONCLUSION

This work presented IWoL, a unified representation-learning and communication framework for cooperative MARL. This learns a compact latent that jointly captures inter-agent relations and privileged task information through a representation-oriented communication protocol. Extensive experiments show that IWoL variants attain best performance in 10 out of 10 robotic tasks.

Closing Remarks: One especially appealing property of IWoL is its **versatility**—allowing practitioners to toggle between message-free (implicit) and message-rich (explicit) coordination without additional modules. Given the notorious sensitivity of large-scale MARL, we believe that offering a drop-in solution that is both *efficient and simple* is a timely contribution to the community.

FUTURE DIRECTIONS

Recently, generalizability has been a key challenge in the machine learning domain, and its promising workaround is representation learning, achieving notable success in real-world applications, *e.g.*, foundation and omni models (Black et al., 2024; Intelligence et al., 2025). For single-agent RL, diverse representation learning methods have been introduced, *e.g.*, successor features (Agarwal et al., 2024; Sikchi et al., 2024; Barreto et al., 2017), forward-backward representations (Touati & Ollivier, 2021; Touati et al., 2022), quasimetrics (Wang et al., 2023; Valieva & Banerjee, 2024), bisimulation (Zhang et al., 2020; Kemertas & Aumentado-Armstrong, 2021; Hansen-Estruch et al., 2022), temporal distance (Park et al., 2024; Bae et al., 2024; Lee & Kwon, 2025b), and contrastive objectives (Zheng et al., 2023; Myers et al., 2024), each contributing to more generalizable RL agents.

Unlike the single-agent setting, where representations can be extracted from a fully observable environment, extending this perspective to MARL is not a trivial problem. That is because MARL requires handling diverse information such as inter-agent relationships, their role structures, and shared world dynamics under a partially observable MDP. While some methods leverage one of these aspects in isolation, there has been limited progress in integrating them into a unified representation that captures the factors facilitating team coordination. Alternatively, to develop the generalizability, ad-hoc teamwork (Wang et al., 2024a; Gu et al., 2022) and zero-shot adaptation (Jha et al., 2025) have highlighted the importance of enabling agents to coordinate with previously unseen partners. They suggest that increasing the diversity of self-play scenarios can improve agents’ adaptation and generalization ability.

While our approach is not designed as a direct solution to these challenges, it provides a unified latent representation that could support such functionalities. From this perspective, we envision several meaningful directions for future research:

- How can we leverage a representation learning framework from a single-agent to a multi-agent setting?
- Can we construct an omni-representation that jointly encodes diverse information in a scalable manner?
- What information and mechanisms facilitate rapid role alignment and policy adaptation in multi-agent dynamics?

In conclusion, this work is an initial step toward bridging representation learning and generalizable multi-agent coordination, instead of attempting a definitive solution to these open challenges. Our framework provides a foundation upon which future work can build more adaptive and versatile strategies using a unified latent representation. Finally, we hope this perspective stimulates further exploration into *omni-representation* and its role in enabling robust open-world multi-agent systems.

REFERENCES

- Siddhant Agarwal, Harshit Sikchi, Peter Stone, and Amy Zhang. Proto successor measure: Representing the space of all possible solutions of reinforcement learning. *arXiv preprint arXiv:2411.19418*, 2024.
- Junik Bae, Kwanyoung Park, and Youngwoon Lee. TLDR: Unsupervised goal-conditioned RL via temporal distance-aware representations. *arXiv preprint arXiv:2407.08464*, 2024.
- Simon Baron. *Mindblindness: An essay on autism and theory of mind*. MIT press, 1997.
- André Barreto, Will Dabney, Rémi Munos, Jonathan J Hunt, Tom Schaul, Hado P van Hasselt, and David Silver. Successor features for transfer in reinforcement learning. *NeurIPS*, 30, 2017.
- Daniel S Bernstein, Robert Givan, Neil Immerman, and Shlomo Zilberstein. The complexity of decentralized control of Markov decision processes. *Mathematics of operations research*, 27(4): 819–840, 2002.
- Kevin Black, Noah Brown, Danny Driess, Adnan Esmail, Michael Equi, Chelsea Finn, Niccolo Fusai, Lachy Groom, Karol Hausman, Brian Ichter, et al. π_0 : A vision-language-action flow model for general robot control. *arXiv preprint arXiv:2410.24164*, 2024.

- Yang Cai, Xiangyu Liu, Argyris Oikonomou, and Kaiqing Zhang. Provable partially observable reinforcement learning with privileged information. *NeurIPS*, 37:63790–63857, 2024.
- Yuanpei Chen, Tianhao Wu, Shengjie Wang, Xidong Feng, Jiechuan Jiang, Zongqing Lu, Stephen McAleer, Hao Dong, Song-Chun Zhu, and Yaodong Yang. Towards human-level bimanual dexterous manipulation with reinforcement learning. In *NeurIPS*, 2022.
- Phillip JK Christoffersen, Andrew C Li, Rodrigo Toro Icarte, and Sheila A McIlraith. Learning symbolic representations for reinforcement learning of non-markovian behavior. *arXiv preprint arXiv:2301.02952*, 2023.
- Allan Dafoe, Edward Hughes, Yoram Bachrach, Tantum Collins, Kevin R McKee, Joel Z Leibo, Kate Larson, and Thore Graepel. Open problems in cooperative AI. *arXiv preprint arXiv:2012.08630*, 2020.
- Jilles Dibangoye and Olivier Buffet. Learning to act in decentralized partially observable MDPs. In *ICML*, 2018.
- Ziluo Ding, Tiejun Huang, and Zongqing Lu. Learning individually inferred communication for multi-agent cooperation. *NeurIPS*, 2020.
- Prashant Doshi, Piotr Gmytrasiewicz, and Edmund Durfee. Recursively modeling other agents for decision making: A research perspective. *Artificial Intelligence*, 279:103202, 2020.
- Zehao Dou, Jakub Grudzien Kuba, and Yaodong Yang. Understanding value decomposition algorithms in deep cooperative multi-agent reinforcement learning. *arXiv preprint arXiv:2202.04868*, 2022.
- Lasse Espeholt, Hubert Soyer, Remi Munos, Karen Simonyan, Vlad Mnih, Tom Ward, Yotam Doron, Vlad Firoiu, Tim Harley, Iain Dunning, et al. IMPALA: Scalable distributed deep-RL with importance weighted actor-learner architectures. In *ICML*, 2018.
- Baofu Fang, Caiming Zheng, and Hao Wang. Fact-based agent modeling for multi-agent reinforcement learning. *arXiv preprint arXiv:2310.12290*, 2023.
- Mingxiao Feng, Wengang Zhou, Yaodong Yang, and Houqiang Li. Joint-predictive representations for multi-agent reinforcement learning. In *OpenReview*, 2023.
- Jakob Foerster, Ioannis Alexandros Assael, Nando De Freitas, and Shimon Whiteson. Learning to communicate with deep multi-agent reinforcement learning. *NeurIPS*, 2016.
- Jakob Foerster, Gregory Farquhar, Triantafyllos Afouras, Nantas Nardelli, and Shimon Whiteson. Counterfactual multi-agent policy gradients. In *AAAI*, 2018.
- Sam Ganzfried and Tuomas Sandholm. Game theory-based opponent modeling in large imperfect-information games. In *AAMAS*, 2011.
- St John Grimby, Jonathan Shock, and Arnu Pretorius. Causal multi-agent reinforcement learning: Review and open problems. *arXiv preprint arXiv:2111.06721*, 2021.
- Niko A Grupen, Daniel D Lee, and Bart Selman. Multi-agent curricula and emergent implicit signaling. *AAMAS*, 2022.
- Pengjie Gu, Mengchen Zhao, Jianye Hao, and Bo An. Online ad hoc teamwork under partial observability. In *ICLR*, 2022.
- Cong Guan, Feng Chen, Lei Yuan, Chenghe Wang, Hao Yin, Zongzhang Zhang, and Yang Yu. Efficient multi-agent communication via self-supervised information aggregation. *Advances in Neural Information Processing Systems*, 2022.
- Nikunj Gupta, Somjit Nath, and Samira Ebrahimi Kahou. CAMMAREL: Conformal action modeling in multi agent reinforcement learning. *arXiv preprint arXiv:2306.11128*, 2023.
- Danijar Hafner, Jurgis Pasukonis, Jimmy Ba, and Timothy Lillicrap. Mastering diverse domains through world models. *Nature*, 2025.

- Philippe Hansen-Estruch, Amy Zhang, Ashvin Nair, Patrick Yin, and Sergey Levine. Bisimulation makes analogies in goal-conditioned reinforcement learning. In *ICML*, pp. 8407–8426. PMLR, 2022.
- He He, Jordan Boyd-Graber, Kevin Kwok, and Hal Daumé III. Opponent modeling in deep reinforcement learning. In *ICML*, 2016.
- Keyang He, Prashant Doshi, and Bikramjit Banerjee. Reinforcement learning in many-agent settings under partial observability. In *UAI*, 2022.
- Trong Nghia Hoang and Kian Hsiang Low. Interactive POMDP Lite: Towards practical planning to predict and exploit intentions for interacting with self-interested agents. *IJCAI*, 2013.
- Edward S Hu, James Springer, Oleh Rybkin, and Dinesh Jayaraman. Privileged sensing scaffolds reinforcement learning. *arXiv preprint arXiv:2405.14853*, 2024a.
- Shengchao Hu, Li Shen, Ya Zhang, and Dacheng Tao. Communication learning in multi-agent systems from graph modeling perspective. *ICLR*, 2024b.
- Zican Hu, Zongzhang Zhang, Huaxiong Li, Chunlin Chen, Hongyu Ding, and Zhi Wang. Attention-guided contrastive role representations for multi-agent reinforcement learning. In *ICLR*, 2024c.
- Dongchi Huang, Jiaqi Wang, Yang Li, Chunhe Xia, Tianle Zhang, and Kaige Zhang. PIGDreamer: Privileged information guided world models for safe partially observable reinforcement learning. *ICML*, 2025.
- Peter Huber. Robust estimation of a location parameter. In *Breakthroughs in statistics: Methodology and distribution*. Springer, 1992.
- Dom Huh and Prasant Mohapatra. Representation learning for efficient deep multi-agent reinforcement learning. *arXiv preprint arXiv:2406.02890*, 2024.
- Physical Intelligence, Kevin Black, Noah Brown, James Darpinian, Karan Dhabalia, Danny Driess, Adnan Esmail, Michael Equi, Chelsea Finn, Niccolo Fusai, et al. $\pi_{0.5}$: a vision-language-action model with open-world generalization. *arXiv preprint arXiv:2504.16054*, 2025.
- Kunal Jha, Wilka Carvalho, Yancheng Liang, Simon S Du, Max Kleiman-Weiner, and Natasha Jaques. Cross-environment cooperation enables zero-shot multi-agent coordination. *arXiv preprint arXiv:2504.12714*, 2025.
- Jiechuan Jiang and Zongqing Lu. Learning attentional communication for multi-agent cooperation. *NeurIPS*, 2018.
- Pierre-Alexandre Kamienny, Kai Arulkumaran, Feryal Behbahani, Wendelin Boehmer, and Simon Whiteson. Privileged information dropout in reinforcement learning. *arXiv preprint arXiv:2005.09220*, 2020.
- Sehyeok Kang, Yongsik Lee, Gahee Kim, Song Chong, and Se-Young Yun. $Ma^2 e$: Addressing partial observability in multi-agent reinforcement learning with masked auto-encoder. In *ICLR*, 2025.
- Mete Kemertas and Tristan Aumentado-Armstrong. Towards robust bisimulation metric learning. *NeurIPS*, 34:4764–4777, 2021.
- Jung In Kim, Young Jae Lee, Jongkook Heo, Jinhyeok Park, Jaehoon Kim, Sae Rin Lim, Jinyong Jeong, and Seoung Bum Kim. Sample-efficient multi-agent reinforcement learning with masked reconstruction. *PLoS one*, 18(9), 2023.
- Diederik P Kingma and Jimmy Ba. Adam: A method for stochastic optimization. *ICLR*, 2014.
- Anastasia Koloskova, Hadrien Hendriks, and Sebastian U Stich. Revisiting gradient clipping: Stochastic bias and tight convergence guarantees. In *ICML*, 2023.

- Mikel Landajuela, Brenden K Petersen, Sookyung Kim, Claudio P Santiago, Ruben Glatt, Nathan Mundhenk, Jacob F Pettit, and Daniel Faissol. Discovering symbolic policies with deep reinforcement learning. In *ICML*, 2021.
- Dongsu Lee and Minhae Kwon. Episodic future thinking mechanism for multi-agent reinforcement learning. *NeurIPS*, 2024a.
- Dongsu Lee and Minhae Kwon. Instant inverse modeling of stochastic driving behavior with deep reinforcement learning. *IEEE Transactions on Consumer Electronics*, 2024b.
- Dongsu Lee and Minhae Kwon. Episodic future thinking with offline reinforcement learning for autonomous driving. *IEEE Internet of Things Journal*, 2025a.
- Dongsu Lee and Minhae Kwon. Temporal distance-aware transition augmentation for offline model-based reinforcement learning. *ICML*, 2025b.
- Pascal Leroy, Pablo G Morato, Jonathan Pisane, Athanasios Kolios, and Damien Ernst. IMP-MARL: a suite of environments for large-scale infrastructure management planning via MARL. *NeurIPS*, 2023.
- Dapeng Li, Zhiwei Xu, Bin Zhang, and Guoliang Fan. From explicit communication to tacit cooperation: A novel paradigm for cooperative marl. *arXiv preprint arXiv:2304.14656*, 2023.
- Jiahui Li, Kun Kuang, Baoxiang Wang, Furui Liu, Long Chen, Fei Wu, and Jun Xiao. Shapley counterfactual credits for multi-agent reinforcement learning. In *KDD*, 2021a.
- Jiahui Li, Kun Kuang, Baoxiang Wang, Furui Liu, Long Chen, Changjie Fan, Fei Wu, and Jun Xiao. Deconfounded value decomposition for multi-agent reinforcement learning. In *ICML*, 2022a.
- Qingyao Li, Wei Xia, Li'ang Yin, Jiarui Jin, and Yong Yu. Privileged knowledge state distillation for reinforcement learning-based educational path recommendation. In *KDD*, pp. 1621–1630, 2024a.
- Quanyi Li, Zhenghao Peng, Lan Feng, Qihang Zhang, Zhenghai Xue, and Bolei Zhou. Metadrive: Composing diverse driving scenarios for generalizable reinforcement learning. *IEEE Transactions on Pattern Analysis and Machine Intelligence*, 2022b.
- Sheng Li, Jayesh K Gupta, Peter Morales, Ross Allen, and Mykel J Kochenderfer. Deep implicit coordination graphs for multi-agent reinforcement learning. *AAMAS*, 2021b.
- Xinran Li and Jun Zhang. Context-aware communication for multi-agent reinforcement learning. *AAMAS*, 2024.
- Xinran Li, Zifan Liu, Shibo Chen, and Jun Zhang. Individual contributions as intrinsic exploration scaffolds for multi-agent reinforcement learning. *ICML*, 2024b.
- Zhiyuan Liu, Yankai Lin, and Maosong Sun. *Representation learning for natural language processing*. Springer Nature, 2023.
- Ryan Lowe, Yi I Wu, Aviv Tamar, Jean Harb, OpenAI Pieter Abbeel, and Igor Mordatch. Multi-agent actor-critic for mixed cooperative-competitive environments. *NeurIPS*, 2017.
- Yecheng Jason Ma, Shagun Sodhani, Dinesh Jayaraman, Osbert Bastani, Vikash Kumar, and Amy Zhang. VIP: Towards universal visual reward and representation via value-implicit pre-training. *ICLR*, 2023.
- Viktor Makoviychuk, Lukasz Wawrzyniak, Yunrong Guo, Michelle Lu, Kier Storey, Miles Macklin, David Hoeller, Nikita Rudin, Arthur Allshire, Ankur Handa, et al. Isaac gym: High performance gpu-based physics simulation for robot learning. *arXiv preprint arXiv:2108.10470*, 2021.
- Kinal Mehta, Anuj Mahajan, and Pawan Kumar. Effects of spectral normalization in multi-agent reinforcement learning. In *IJCNN*, 2023.
- Vivek Myers, Chongyi Zheng, Anca Dragan, Sergey Levine, and Benjamin Eysenbach. Learning temporal distances: Contrastive successor features can provide a metric structure for decision-making. *arXiv preprint arXiv:2406.17098*, 2024.

- Kamal K Ndousse, Douglas Eck, Sergey Levine, and Natasha Jaques. Emergent social learning via multi-agent reinforcement learning. In *ICML*, 2021.
- Dung Nguyen, Svetha Venkatesh, Phuoc Nguyen, and Truyen Tran. Theory of mind with guilt aversion facilitates cooperative reinforcement learning. In *ACML*, 2020.
- Yaru Niu, Rohan R Paleja, and Matthew C Gombolay. Multi-agent graph-attention communication and teaming. In *AAMAS*, 2021.
- Ini Oguntola, Joseph Campbell, Simon Stepputtis, and Katia Sycara. Theory of mind as intrinsic motivation for multi-agent reinforcement learning. *ICML ToM Workshop*, 2023.
- Shayegan Omidshafiei, Jason Pazis, Christopher Amato, Jonathan P How, and John Vian. Deep decentralized multi-task multi-agent reinforcement learning under partial observability. In *ICML*, 2017.
- Seohong Park, Tobias Kreiman, and Sergey Levine. Foundation policies with Hilbert representations. *ICML*, 2024.
- Karl Pertsch, Youngwoon Lee, and Joseph Lim. Accelerating reinforcement learning with learned skill priors. In *CoRL*, 2021.
- Daniel Pickem, Paul Glotfelter, Li Wang, Mark Mote, Aaron Ames, Eric Feron, and Magnus Egerstedt. The robotarium: A remotely accessible swarm robotics research testbed. In *ICRA*, 2017.
- Rafael Pina, Varuna De Silva, Corentin Artaud, and Xiaolan Liu. Fully independent communication in multi-agent reinforcement learning. *AAMAS*, 2024.
- David Premack and Guy Woodruff. Does the chimpanzee have a theory of mind? *Behavioral and Brain Sciences*, 1(4):515–526, 1978.
- Guannan Qu, Yiheng Lin, Adam Wierman, and Na Li. Scalable multi-agent reinforcement learning for networked systems with average reward. *NeurIPS*, 2020.
- Neil Rabinowitz, Frank Perbet, Francis Song, Chiyuan Zhang, SM Ali Eslami, and Matthew Botvinick. Machine theory of mind. In *ICML*, 2018.
- Tabish Rashid, Mikayel Samvelyan, Christian Schroeder De Witt, Gregory Farquhar, Jakob Foerster, and Shimon Whiteson. Monotonic value function factorisation for deep multi-agent reinforcement learning. *Journal of Machine Learning Research*, 21(178):1–51, 2020.
- Byungseok Roh, Wuhyun Shin, Ildoo Kim, and Sungwoong Kim. Spatially consistent representation learning. In *CVPR*, 2021.
- Sasha Salter, Dushyant Rao, Markus Wulfmeier, Raia Hadsell, and Ingmar Posner. Attention-privileged reinforcement learning. In *CoRL*, pp. 394–408, 2021.
- John Schulman, Filip Wolski, Prafulla Dhariwal, Alec Radford, and Oleg Klimov. Proximal policy optimization algorithms. *arXiv preprint arXiv:1707.06347*, 2017.
- Wenling Shang, Lasse Espeholt, Anton Raichuk, and Tim Salimans. Agent-centric representations for multi-agent reinforcement learning. *arXiv preprint arXiv:2104.09402*, 2021.
- Jianzhun Shao, Yun Qu, Chen Chen, Hongchang Zhang, and Xiangyang Ji. Counterfactual conservative q learning for offline multi-agent reinforcement learning. In *NeurIPS*, 2023.
- Samuel Shaw, Emerson Wenzel, Alexis Walker, and Guillaume Sartoretti. ForMIC: Foraging via multiagent RL with implicit communication. *IEEE Robotics and Automation Letters*, 7(2):4877–4884, 2022.
- Harshit Sikchi, Siddhant Agarwal, Pranaya Jajoo, Samyak Parajuli, Caleb Chuck, Max Rudolph, Peter Stone, Amy Zhang, and Scott Niekum. RLZero: Direct policy inference from language without in-domain supervision. *arXiv preprint arXiv:2412.05718*, 2024.

- Amanpreet Singh, Tushar Jain, and Sainbayar Sukhbaatar. Learning when to communicate at scale in multiagent cooperative and competitive tasks. *ICLR*, 2019.
- Haolin Song, Mingxiao Feng, Wengang Zhou, and Houqiang Li. MA2CL: masked attentive contrastive learning for multi-agent reinforcement learning. In *IJCAI*, 2023.
- Roland Stolz, Hanna Krasowski, Jakob Thumm, Michael Eichelbeck, Philipp Gassert, and Matthias Althoff. Excluding the irrelevant: Focusing reinforcement learning through continuous action masking. In *NeurIPS*, 2024.
- Sainbayar Sukhbaatar, Rob Fergus, et al. Learning multiagent communication with backpropagation. *NeurIPS*, 2016.
- Jingbo Sun, Songjun Tu, Haoran Li, Xin Liu, Yaran Chen, Ke Chen, Dongbin Zhao, et al. Unsupervised zero-shot reinforcement learning via dual-value forward-backward representation. In *ICLR*, 2025.
- Yanchao Sun, Ruijie Zheng, Parisa Hassanzadeh, Yongyuan Liang, Soheil Feizi, Sumitra Ganesh, and Furong Huang. Certifiably robust policy learning against adversarial multi-agent communication. In *ICLR*, 2023.
- Ahmed Touati and Yann Ollivier. Learning one representation to optimize all rewards. *NeurIPS*, 34: 13–23, 2021.
- Ahmed Touati, J  r  my Rapin, and Yann Ollivier. Does zero-shot reinforcement learning exist? *arXiv preprint arXiv:2209.14935*, 2022.
- Khadichabonu Valieva and Bikramjit Banerjee. Quasimetric value functions with dense rewards. *arXiv preprint arXiv:2409.08724*, 2024.
- Petar Veli  kovi  , Guillem Cucurull, Arantxa Casanova, Adriana Romero, Pietro Lio, and Yoshua Bengio. Graph attention networks. *ICLR*, 2018.
- Caroline Wang, Muhammad Arrasy Rahman, Ishan Durugkar, Elad Liebman, and Peter Stone. N-agent ad hoc teamwork. *NeurIPS*, 2024a.
- Han Wang, Binbin Chen, Tieying Zhang, and Baoxiang Wang. Learning to communicate through implicit communication channels. In *ICLR*, 2024b.
- Han Wang, Binbin Chen, Tieying Zhang, and Baoxiang Wang. Learning to construct implicit communication channel. *ICLR*, 2025.
- Tonghan Wang, Jianhao Wang, Chongyi Zheng, and Chongjie Zhang. Learning nearly decomposable value functions via communication minimization. *ICLR*, 2020.
- Tongzhou Wang, Antonio Torralba, Phillip Isola, and Amy Zhang. Optimal goal-reaching reinforcement learning via quasimetric learning. In *ICML*, 2023.
- Yuanfei Wang, Fangwei Zhong, Jing Xu, and Yizhou Wang. ToM2C: Target-oriented multi-agent communication and cooperation with theory of mind. *ICLR*, 2022.
- Zizhao Wang, Jiaheng Hu, Caleb Chuck, Stephen Chen, Roberto Mart  n-Mart  n, Amy Zhang, Scott Niekum, and Peter Stone. SkiLD: Unsupervised skill discovery guided by factor interactions. *NeurIPS*, 2024c.
- Lawrence G Weiss, Thomas Oakland, and Glen P Aylward. *Bayley-III clinical use and interpretation*. Academic Press, 2010.
- Muning Wen, Jakub Kuba, Runji Lin, Weinan Zhang, Ying Wen, Jun Wang, and Yaodong Yang. Multi-agent reinforcement learning is a sequence modeling problem. *NeurIPS*, 2022.
- Annie Xie, Dylan Losey, Ryan Tolsma, Chelsea Finn, and Dorsa Sadigh. Learning latent representations to influence multi-agent interaction. In *CoRL*, 2021.

- Ziyan Xiong, Bo Chen, Shiyu Huang, Wei-Wei Tu, Zhaofeng He, and Yang Gao. MQE: Unleashing the power of interaction with multi-agent quadruped environment. In *IROS*, 2024.
- Min Yang, Guanjun Liu, Ziyuan Zhou, and Jiacun Wang. Partially observable mean field multi-agent reinforcement learning based on graph attention network for uav swarms. *Drones*, 7(7):476, 2023.
- Chao Yu, Akash Velu, Eugene Vinitzky, Jiaxuan Gao, Yu Wang, Alexandre Bayen, and Yi Wu. The surprising effectiveness of PPO in cooperative multi-agent games. *NeurIPS*, 2022a.
- Xiaopeng Yu, Jiechuan Jiang, Wanpeng Zhang, Haobin Jiang, and Zongqing Lu. Model-based opponent modeling. *NeurIPS*, 2022b.
- Lei Yuan, Jianhao Wang, Fuxiang Zhang, Chenghe Wang, Zongzhang Zhang, Yang Yu, and Chongjie Zhang. Multi-agent incentive communication via decentralized teammate modeling. In *AAAI*, 2022.
- Lei Yuan, Ziqian Zhang, Lihe Li, Cong Guan, and Yang Yu. A survey of progress on cooperative multi-agent reinforcement learning in open environment. *arXiv preprint arXiv:2312.01058*, 2023.
- Amy Zhang, Rowan McAllister, Roberto Calandra, Yarin Gal, and Sergey Levine. Learning invariant representations for reinforcement learning without reconstruction. *arXiv preprint arXiv:2006.10742*, 2020.
- Kaiqing Zhang, Zhuoran Yang, and Tamer Başar. Multi-agent reinforcement learning: A selective overview of theories and algorithms. *Handbook of reinforcement learning and control*, pp. 321–384, 2021.
- Zhuoya Zhao, Enmeng Lu, Feifei Zhao, Yi Zeng, and Yuxuan Zhao. A brain-inspired theory of mind spiking neural network for reducing safety risks of other agents. *Frontiers in neuroscience*, 16: 753900, 2022.
- Chongyi Zheng, Ruslan Salakhutdinov, and Benjamin Eysenbach. Contrastive difference predictive coding. *arXiv preprint arXiv:2310.20141*, 2023.
- Zhengbang Zhu, Minghuan Liu, Liyuan Mao, Bingyi Kang, Minkai Xu, Yong Yu, Stefano Ermon, and Weinan Zhang. MADIFF: Offline multi-agent learning with diffusion models. *NeurIPS*, 2024.
- Jennifer M Zubler, Lisa D Wiggins, Michelle M Macias, Toni M Whitaker, Judith S Shaw, Jane K Squires, Julie A Pajek, Rebecca B Wolf, Karnesha S Slaughter, Amber S Broughton, et al. Evidence-informed milestones for developmental surveillance tools. *Pediatrics*, 149(3), 2022.

Appendix: Learning to Interact in World Latent for Team Coordination

CONTENTS

A	Miscellaneous	18
A.1	Summary of Notations	18
A.2	System Specification	18
B	Extensive Related Works	19
B.1	Usage differences of Transformer in MAT, CommFormer, and IWoL	19
B.2	Implicit communication as inverse modeling	19
B.3	Privileged Information in Learning to Control	20
C	Training Details	21
C.1	Pseudocode for IWoL	21
C.2	Implementation Details	22
D	Toy Example Details	23
E	Experimental Details	24
E.1	MetaDrive	24
E.2	Robotarium	25
E.3	Multi-agent Quadruped Environments	26
E.4	Bi-DexHands	28
E.5	Hyperparameters	30
E.6	Baseline Algorithms	30
F	Additional Results	31
F.1	Ablation Study	31
F.2	Training Time	31
F.3	Inference Time at Deployment	32
F.4	Comparison with ICP	32
F.5	IWoL with Off-policy Family Algorithm	33
F.6	Full Training Curve	33

A MISCELLANEOUS

A.1 SUMMARY OF NOTATIONS

Dec-POMDP elements

Notation	Description	Notation	Description
\mathcal{I}	agents set	i	agent index
I	the number of agents	$\gamma \in [0, 1)$	discount factor
\mathcal{S}	state space	s^t	state
\mathcal{O}_i	observation space of agent i	o_i^t	local observation of agent i
\mathcal{A}_i	action space of agent i	a_i^t	action of agent i
\mathcal{T}	state transition model	Ω_i	observation function of agent i
r_i	reward function for agent i	R_i^t	Return of agent i

Algorithm elements

Notation	Description	Notation	Description
M_i^0	space of initialized messages	M_i	space of processed messages
$m_i^{t(0)}$	initialized message from agent i	m_i^t	final processed message for agent i
$m_i^{t(l)}$	message for agent i at round l	L	total communication rounds
f_i^t	intermediate embedding of agent i	$g_{i,j}^t$	relationship between agents i and j
G^t	topology graph	a_{gg}	weighting vector of the additive attention
z_i^t	interactive world latent for agent i	s_i^t	privileged state for agent i
\hat{m}_i^t	reproduced message of agent i	\hat{s}_i^t	reproduced privileged state of agent i

RL Training

Notation	Description	Notation	Description
ϕ_i	policy parameters for agent i	θ	value function parameters
λ_W	balancing coefficient for world latent loss	λ_I	balancing coefficient for interactive latent loss
ϵ	clip coefficient of PPO loss	δ	threshold of Huber loss
K	the number of updates	T	max steps of an episode
B	batch size	\mathcal{D}	online replay buffer
η	learning rate		

A.2 SYSTEM SPECIFICATION

CPU	AMD EPYC 7713 64-Core
GPU	RTX A6000 & A5000
Software	CUDA: 11.8, cudnn: 8.7.0, python: 3.8
PyTorch	2.1.0 (MetaDrive), 2.0.1 (Robotarium), 2.4.1 (MQE and Bi-hand Dexterous)

B EXTENSIVE RELATED WORKS

B.1 USAGE DIFFERENCES OF TRANSFORMER IN MAT, COMMFORMER, AND IWOL

MAT (Wen et al., 2022) first formulates cooperative MARL as a sequence modeling problem, employing a full encoder–decoder Transformer to map a sequence of agents’ joint observations to a sequence of optimal actions. The encoder uses stacked self-attention and MLP blocks to capture high-level inter-agent dependencies, while the decoder generates each agent’s action auto-regressively under a causal mask that restricts attention to preceding agents. This design yields linear complexity in the number of agents and comes with a monotonic performance improvement guarantee.

CommFormer (Hu et al., 2024b) basically builds on MAT by explicitly learning a sparse communication graph. It introduces a learnable adjacency matrix and incorporates this graph both as an explicit edge embedding in the attention score computation and as a hard mask to gate message passing. Consequently, its Transformer encoder and decoder are conditioned on both causal order and dynamic connectivity, enabling concurrent optimization of communication architecture and policy parameters in an end-to-end fashion.

In IWOL, the Transformer block is repurposed exclusively as the communication processor, instead of a policy or value function. After each agent’s local observation is encoded, a Graph-Attention Transformer applies multi-head scaled dot-product attention over a communication graph to refine interactive embeddings.

We summarize the usage differences of the Transformer in these methods as follows.

- MAT: Transformer serves as the joint policy network, with encoder–decoder modeling and causal masking.
- CommFormer: Transformer integrated with a learnable, sparsity-controlled communication graph to gate attention.
- IWOL: First work to design the communication processor itself as a graph-attention Transformer, combining attention-based message encoding.

B.2 IMPLICIT COMMUNICATION AS INVERSE MODELING

Implicit communication channel. A growing body of work has explored implicit coordination without explicit messaging. For example, (Li et al., 2023) trains agents to gradually shift from using explicit messages to purely tacit cooperation. Other approaches learn latent coordination through structured interactions, such as inferring dynamic coordination graphs, or via environment-mediated signaling (Li et al., 2021b). Notably, some methods endow agents with implicit communication abilities by leveraging shared environment cues (Wang et al., 2024b; Shaw et al., 2022; Grupen et al., 2022; Wang et al., 2025). However, these implicit communication frameworks typically lack a dedicated learned messaging architecture and often focus on narrow aspects of coordination, which is similar to inverse modeling through environmental to behavioral cues.

Machine theory of mind. Another line of research draws on cognitive reasoning (Baron, 1997; Premack & Woodruff, 1978), where agents explicitly model each other’s beliefs, intentions, or roles. For example, theory-of-mind (ToM) approaches have been combined with social incentives like guilt aversion to encourage cooperation (Rabinowitz et al., 2018; Nguyen et al., 2020; Leroy et al., 2023). Such agents maintain internal beliefs about what others will do and even what others believe they will do, implementing recursive reasoning to adjust their policies (Wang et al., 2022; Oguntola et al., 2023; Doshi et al., 2020). Similarly, brain-inspired ToM models use structured networks with dedicated modules for perspective-taking, policy inference, and action prediction, that is, essentially mimicking human mentalizing by explicitly predicting others’ observations and actions (Zhao et al., 2022).

Agent modeling and action prediction. A third branch of related work focuses on agents forecasting or simulating their counterparts’ behavior to improve coordination (He et al., 2016; Yu et al., 2022b; Ganzfried & Sandholm, 2011). Recent methods explicitly model other agents’ policies or future actions as part of the decision process. For example, (Gupta et al., 2023) introduces conformal prediction sets to model other agents’ actions with high confidence, providing each agent with a set of likely moves of others before acting. Interactive MDPs explicitly construct recursive belief

models of other agents’ hidden states and policies to guide planning, whereas interactive latent coding methods learn compact embeddings of observed interaction dynamics without forming full belief hierarchies (Xie et al., 2021; Hoang & Low, 2013). Other approaches give agents an explicit planning capability, such as an episodic future thinking mechanism where an agent infers each partner’s latent character and then simulates future trajectories of all agents to select an optimal action (Lee & Kwon, 2024a;b; 2025a). Likewise, fact-based agent modeling trains a dedicated belief inference network that uses an agent’s own observations and rewards to reconstruct the policies of other agents through a variational auto-encoder (Fang et al., 2023). These techniques incorporate additional structures to predict or encode other agents’ states, essentially bolting on an extra layer of agent-specific reasoning.

I_m-IWOL departs from all three lines by folding communication and modeling into a single Transformer block that is used only during centralized training. Messages circulate through the Transformer while the topology and latent code are being learned, but at test time, each agent discards the channel and relies solely on the cached latent embeddings produced by its local encoder; no decoder, simulator, or action-based signalling set is required. This makes $IWOL$, to our knowledge, the first implicit-communication framework that needs zero additional modules at deployment while still endowing agents with an internal world latent that unifies inter-agent relations and global task information. Consequently, I_m-IWOL inherits the bandwidth-free, attack-resistant advantages of prior implicit schemes, yet retains the architectural simplicity and real-time footprint of a feed-forward network.

B.3 PRIVILEGED INFORMATION IN LEARNING TO CONTROL

Privileged information, which is signals available at training but not at deployment, has been widely adopted for learning to control (Cai et al., 2024; Li et al., 2024b; Ndousse et al., 2021; Salter et al., 2021; Hu et al., 2024a; Kamienny et al., 2020; Li et al., 2024a; Huang et al., 2025), *e.g.*, MARL under partial observability, world model training, and policy improvement. For MARL, it has been introduced both as a training-only information for exploration or credit assignment (Cai et al., 2024; Li et al., 2024b; Ndousse et al., 2021), as well as an attention or distillation signal to align decentralized policies with global information (Salter et al., 2021; Li et al., 2024a). For world-model training, privileged sensing has guided the training of latent dynamics and representation alignment to improve sample efficiency and safety (Hu et al., 2024a; Huang et al., 2025). Furthermore, robustness techniques such as privileged information dropout prevent over-reliance on non-deployable signals and encourage policies to learn deployable features (Kamienny et al., 2020). Across these settings, the unifying principle is that privileged signals are leveraged as auxiliary supervision during training, but removed at deployment to ensure fairness and applicability. In our work, we follow this paradigm by using a privileged decoder to align shared latent representations, while keeping execution fully decentralized and based only on local observations.

C TRAINING DETAILS

C.1 PSEUDOCODE FOR IWOL

Algorithm 1 Training IWOL

```

1: Require: the number of episode  $K$ , the number of agents  $I$ , max steps of an episode  $T$ , batch
   size  $B$ , replay buffers  $\mathcal{D}_i$  for each agent  $i$ , and learning rate  $\eta$ 
2: Initialize: actor parameters  $\Phi = \{\phi_1, \phi_2, \dots, \phi_I\}$ , and critic parameters  $\Theta = \{\theta_1, \theta_2, \dots, \theta_I\}$ 
3: Initialize buffer  $\mathcal{D}_i$  and loss function  $\mathcal{L}(\theta_i), \mathcal{L}(\phi_i)$ 
4: for episode = 1,  $K$  do
5:   Reset privileged state  $s$ , observations  $\mathbf{o}$ 
6:   # Roll-out trajectories -----
7:   for  $t = 1, T_{\max}$  do
8:     Local observation embedding:  $\mathbf{f}^t, \mathbf{m}^{t,0} \leftarrow \text{Encoder}(\text{SelfAttn}(\mathbf{o}))$ 
9:     Scheduling communication:  $G^t \leftarrow \text{GumbelSoftmax}(\text{AddAtt}(\mathbf{f}^t))$ 
10:    Message processing with  $L$  hops:  $\mathbf{m}^t \leftarrow \text{Transformer}(\mathbf{m}^{t,0}, G^t, L)$ 
11:    # Building latent for coordination -----
12:    Im-IWoL:  $\mathbf{z}^t \leftarrow \text{Interactive World Encoder}(\mathbf{f}^t)$  # Ex-IWoL:  $\mathbf{z}^t \leftarrow \mathbf{m}^t$ 
13:    # Policy and Value Function -----
14:    Im-IWoL:  $\mathbf{a}^t \leftarrow \Pi_{\Phi}(\mathbf{z}^t)$  and  $\mathbf{v}^t \leftarrow \mathbf{V}_{\Theta}(\mathbf{m}^t, \mathbf{f}^t)$  # Ex-IWoL:  $\mathbf{a}^t \leftarrow \Pi_{\Phi}(\mathbf{z}^t, \mathbf{f}^t)$ 
15:    Perform action  $\mathbf{a}^t$ , then transit state  $s^{t+1}$ , receive  $\mathbf{r}^t$  and  $\mathbf{o}^{t+1}$ 
16:    Store transition  $(o_i^t, a_i^t, \pi_{\phi_i}(a_i^t|o_i^t), V_{\theta_i}(o_i^t), o_i^{t+1})$  in  $\mathcal{D}_i$  for each agent  $i$ 
17:     $t \leftarrow t + 1$ 
18:  end for
19:  # Return estimation -----
20:  for  $i = 1, I$  do
21:    for  $t = 1, T_{\max}$  do
22:       $R_i^t = r_i^t + \gamma R_i^{t+1}$  if  $o_i^{t+1} \neq \text{terminal}$  from  $\mathcal{D}_i$ 
23:    end for
24:    # Decentralized network update -----
25:    Reconstruct privileged state:  $\hat{s}_i^t \leftarrow \text{Decoder}_W(z_i^t)$ 
26:    Calculate  $\mathcal{L}_{\text{World}} \leftarrow \lambda_W \cdot \text{MSE}(s_i^t, \hat{s}_i^t)$ 
27:    Reconstruct communication message:  $\hat{m}_i^t \leftarrow \text{Decoder}_I(z_i^t)$  # only Im-IWoL
28:    Calculate  $\mathcal{L}_{\text{Interactive}} \leftarrow \lambda_I \cdot \text{MSE}(m_i^t, \hat{m}_i^t)$  # Ex-IWoL,  $\mathcal{L}_{\text{Interactive}} = 0$ 
29:    Calculate  $\mathcal{L}(\phi_i)$  and  $\mathcal{L}(\theta_i)$  using  $\mathcal{D}_i$  with equation 1 and equation 2
30:     $\mathcal{L}(\phi_i) \leftarrow \mathcal{L}(\phi_i) + \mathcal{L}_{\text{Interactive}} + \mathcal{L}_{\text{World}}$ 
31:    Update  $\theta_i \leftarrow \theta_i - \eta \nabla \mathcal{L}(\theta_i)$  and  $\phi_i \leftarrow \phi_i - \eta \nabla \mathcal{L}(\phi_i)$ 
32:  end for
33:  episode  $\leftarrow$  episode + 1
34: end for

```

C.2 IMPLEMENTATION DETAILS

Multi-threaded synchronous policy optimization. Our training implementation employs N_{threads} parallel worker threads, each running an independent environment and collecting fixed-length trajectory segments (Singh et al., 2019). After each segment, every worker computes policy and value function losses to derive gradients, which are then synchronously aggregated across all threads. We average these gradients and perform a single parameter update using the Adam optimizer (Kingma & Ba, 2014). To promote exploration, we include an entropy bonus with weight 0.01 and train the value head with a mean-squared error loss (Schulman et al., 2017). Gradients are clipped to a maximum norm of 0.5 to ensure stable updates (Koloskova et al., 2023). Updated network parameters are then broadcast back to all workers before the next rollout cycle.

Decentralized value function for IWOL variants. In our approach, we adopt privileged state information for each agent, enabling it to alleviate heavy dependence on a centralized critic in previous methods. Consequently, every agent learns its own value function in a fully decentralized fashion (*i.e.*, using only its local, augmented observations) thereby avoiding the communication overhead and staleness issues inherent to a centralized value estimate, while still benefiting from the extra privileged information to maintain sample efficiency and training stability.

Training Details. Additionally, we employ two techniques for efficient updates: value normalization (Mehta et al., 2023) and active masking (Stolz et al., 2024). Value normalization keeps the target values R_i^t on a consistent scale, improving stability and training convergence. Next, optionally employ active masks in the critic to ensure that irrelevant states or features do not excessively affect the value function estimates. This can help the critic focus on relevant state dimensions and reduce training variance.

Fairness of Baseline Implementation. To ensure a fair comparison, we modify some practical implementations of all baselines so as to IWOL:

- **Use of privileged/global information:** Every CTDE baseline (MAPPO, MAT, MAGIC, CommFormer) was given access to the exact same privileged signal, either the ground-truth global state s^t or the concatenated shared observation $\mathbf{o}^t = [o_1^t, \dots, o_n^t]$, when fitting its value function. In other words, *all* methods can use the same global information in a training phase, so that any performance gap cannot be attributed to unequal access to global information.
- **Local-observation encoding:** To match IWOL’s encoder capacity, we equipped each baseline with an identical local-observation embedding pipeline: each agent’s raw observation o_i^t is first projected into a fixed-dimensional feature, then passed through a self-attention layer or a lightweight RNN. We held all embedding hyperparameters constant across methods. This design guarantees that improvements stem from our communication–world-latent architecture rather than from extra encoding power.
- **Hyperparameter:** To ensure a fair comparison, we aligned both algorithmic and environment parameters across all methods. For algorithmic hyperparameters, we adopted the original settings reported in each paper (*i.e.*, learning rates, network architectures, PPO-dependent parameters such as clipping ϵ , value-loss, and entropy weights). In addition, we fixed batch size, hidden dimensions, number of attention heads, and all PPO-specific coefficients to be identical for IWOL and every baseline. Next, for environmental hyperparameters, all training parameters, *e.g.*, maximum episode length, reward scaling, observation noise, and number of parallel environments, were standardized across experiments.

D TOY EXAMPLE DETAILS

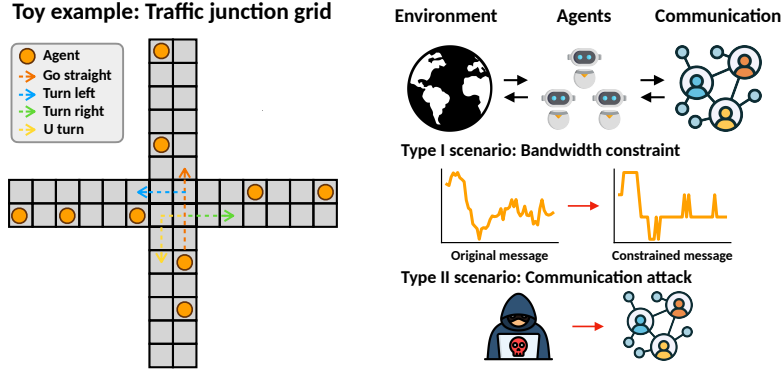


Figure 9: **A diagram for a toy example.** In this example, we adopt a simple traffic junction task and two challenging scenarios in communication MARL.

Simple Traffic Junction. We consider a 4-way traffic junction on a 14×14 grid. At each time step, new cars enter from each of the four entry points with probability p_{arrive} , up to a maximum of $N_{\text{max}} = 10$ concurrent cars. Each car occupies a single cell and is randomly assigned one of four routes (keeping to the right side): straight, left turn, right turn, or U turn. At each step, an agent chooses between two actions: moving one cell or staying in place.

Agents aim to exit the grid upon reaching their destination. They can get a one-hot encoding of its route ID $(\{n, l, r\})$ as an observation without others’ information. Agents overcome their partial observability by explicitly communicating with all others.

The total team reward at time t is as follows:

$$r(t) = C^t r_{\text{coll}} + \sum_{i=1}^{N^t} \tau_i r_{\text{time}},$$

where C^t the number of collisions, N^t the number of cars present, r_{coll} is a collision penalty, r_{time} is a time penalty, and τ is the number of steps since that car entered. Episodes run for 40 steps and are marked as failures if any collision occurs.

Type I: Bandwidth Constraint. In *Type I*, we limit the number of bits used to transmit each continuous message vector m_i^t . Originally, we used 32 bits per element. Here, we quantize to only $n \in \{8, 2\}$ bits per element and measure the resulting performance drop. At execution time, we consider the following bandwidth constraints:

```
def bit_per_sec_const(message, n):
    levels = 2**n
    # scale to [0, levels-1], round, then rescale to [0,1]
    const_m = torch.round(message * (levels - 1)) / (levels - 1)
    return const_m
```

for $n = 8$ (Type I - 8bps) or $n = 2$ (Type I - 2bps).

Type II: Communication Attack. In *Type II*, an adversary intercepts and corrupts each agent’s message before delivery. Concretely, for every transmitted m_i^t , we sample a random vector $\hat{m}_i^t \sim \mathcal{U}$ and deliver \hat{m}_i^t in place of the true message. This simulates a worst-case message corruption scenario, and we report the performance degradation under this attack.

E EXPERIMENTAL DETAILS

This appendix section describes the task and details of a Markov decision process over 10 scenarios.

Remark. Each task requires extensive notation so that some symbols may overlap with those used in the main text. Readers are therefore advised to consult each MDP specification and notation in the context of its own environment.

E.1 METADRIVE

(*Limited observability, high-dimensional observation space, large-scale, cooperative, and competitive*) MetaDrive is an autonomous driving simulator formulated as an MDP. Each vehicle simultaneously learns a driving policy, a value function, and a communication protocol.

E.1.1 MARKOV DECISION PROCESS

Observation. In particular, at each timestep t , agent i receives an observation o_i^t composed of three parts: ego-vehicle information, surrounding vehicles’ information, and navigation cues.

- Ego-vehicle information: $[\theta_i, \phi_i, v_i, d_i^{\text{left}}, d_i^{\text{right}}]$ where θ_i is steering angle, ϕ_i is heading, v_i is speed, and $d_i^{\text{left}}, d_i^{\text{right}}$ are distances to left/right lane boundaries
- Surrounding vehicles’ information: relative positions and velocities of up to N_{obs} nearest agents, sensed via a LiDAR with N_{laser} beams covering a d_{laser} .
- Navigation cues: A vector encoding direction and distance to the destination.

Actions. Each agent selects a continuous action $a_i^t = [\alpha_i^t, \beta_i^t]$, where $\alpha_i^t \in [-1, 1]$ controls steering (left: -1 , right: $+1$), and $\beta_i^t \in [-1, 1]$ controls acceleration (brake: -1 , throttle: $+1$).

Reward. We design the individual reward into three components:

$$r_i^I = c^{\text{driving}} r_i^{\text{driving}} + c^{\text{speed}} r_i^{\text{speed}} + r_i^{\text{termination}},$$

where driving progress r_i^{driving} is the forward distance traveled along the lane between t and $t + 1$, agility reward $r_i^{\text{speed}} = \frac{v_i^t}{v_{\text{max}}}$ normalizes current speed by the maximum allowed v_{max} , and termination reward $r_i^{\text{termination}} = c_{\text{goal}}$ if goal reached (if collision or out-of-lane, $r_i^{\text{termination}} = c_{\text{fail}}$). c_{goal} is always positive, and c_{fail} is set as a negative.

To encourage cooperation, we further define a cooperative reward $r_i^C = \sum_{j \in \mathcal{N}_i} r_j^I$, where \mathcal{N}_i is the set of vehicles within communication range. The total reward is then $r_i = (1 - \lambda_{\text{co}}) r_i^I + \lambda_{\text{co}} r_i^C$, balancing individual performance ($\lambda_{\text{co}} = 0$) and team coordination ($\lambda_{\text{co}} > 0$).

E.1.2 SCENARIO DESCRIPTIONS

We provide two types of driving scenarios, intersection and parking lot. These environments are designed to test the agent’s communication ability in large-scale MARL and the holistic coordination ability of their action, considering safety, goal achieving, and agility.

Intersection: An unprotected four-way intersection without traffic signals. Agents must negotiate right-of-way, decide when to turn or go straight, and avoid gridlock. Explicit communication of intentions (e.g. yield, turn left) reduces ambiguity and improves safety.

Parking Lot: A confined lot with eight parking slots and spawn points both inside and on adjacent roads. Vehicles may need to reverse, yield, or reroute to find a spot. Real-time information exchange helps agents agree on who moves when and where to park without blocking traffic.

E.2 ROBOTARIUM

(*Limited observability, cooperative, and robotics*) The Robotarium platform is a remotely accessible multi-robot lab from Georgia Tech, enabling researchers to conduct physical robot experiments with ease. In this setup, mobile robots that do not have sensors or LiDAR rely on inter-robot communication to coordinate actions, avoid collisions, and stay within bounds. We evaluate our method in two scenarios with four robotic agents: simple navigation and material transport. In such a simple simulator, we test their coordination performance without observation devices.

Simple Navigation: During each episode, the swarm robots navigate toward a destination point that may vary across episodes. Each agent is provided only with its own position and the destination’s coordinates as observations.

In this scenario, privileged state at time t is $\hat{s}^t = \{(x_i^t, y_i^t), (x_i^{\text{goal}}, y_i^{\text{goal}})\}_{i=1}^N$, where (x_i^t, y_i^t) is agent i ’s position and $(x_i^{\text{goal}}, y_i^{\text{goal}})$ is its fixed goal location. Each agent i receives a local observation $o_i^t = [x_i^t, y_i^t, x_i^{\text{goal}}, y_i^{\text{goal}}] \in \mathbb{R}^4$, containing its own coordinates and the coordinates of its goal. After receiving o_i^t , Agents choose from five discrete actions $\mathcal{A} = \{\text{left}, \text{right}, \text{up}, \text{down}, \text{no_action}\}$. A `no_action` leaves the agent in place, and other actions move the agent by a fixed distance d_{step} in the corresponding cardinal direction.

Subsequently, at each timestep, agent i receives a mixed reward as an outcome of a joint action $r_i^t = (1 - \lambda_{co}) r_i^I + \lambda_{co} r_i^G$, where $r_i^I = -\|(x_i^t, y_i^t) - (x_i^{\text{goal}}, y_i^{\text{goal}})\|^2$, $r_i^G = \frac{1}{N-1} \sum_{j \neq i} r_j^I$. An error penalty of -5 is applied if agent i collides with another agent or violates workspace boundaries.

Material Transport: In this scenario, there are two types of swarm robots: slow and fast robots. They aim to move loads from the loading zones to the unloading zone (target). In particular, Figure 6 (g) shows that loading and unloading zones are colored purple and green; orange and red circled robots are slow and fast ones, respectively. To enhance efficiency, these robots need inter-agent communication to coordinate their behaviors for avoiding collision and splitting their workstations (*i.e.*, fast robots move the material from a distant loading area, and slow robots work in close one).

We designed MDP for such a scenario as follows. First, a privileged state at time t is $\hat{s}^t = [\{(x_i^t, y_i^t), l_i^t, \tau_i^t, v_i^t\}_{i=1}^N, z_1^t, z_2^t]$, where (x_i^t, y_i^t) is agent i ’s position, l_i^t is its current load, τ_i^t is its torque, v_i^t is its speed, and z_1^t, z_2^t are the remaining loads at zone 1 and zone 2. Each agent i can get an observation $o_i^t = [x_i^t, y_i^t, l_i^t, z_1^t, z_2^t] \in \mathbb{R}^5$. Agents make a decision within the same action space with the simple navigation scenario. At each timestep, agent i receives the reward as follows:

$$r_i^t = c_{\text{step}} + c_{\text{load-close}}(l_i^t m_{\text{load}}) + c_{\text{load-distant}}(l_i^t m_{\text{load}}) + c_{\text{unload}}(l_i^t m_{\text{unload}}) + c_{\text{safety}} \mathbb{1}_{\text{safety}},$$

where c_{step} is the constant time penalty per step, $c_{\text{load-close}}$ and $c_{\text{load-distant}}$ are the reward coefficient for loading at zone 1 and 2, respectively. Next, c_{unload} is the reward coefficient for unloading at the target area, c_{safety} is the penalty coefficient for safety violations (collision or boundary exit), and $\mathbb{1}_{\text{safety}}$ is an indicator function equal to 1 if a safety event occurs, 0 otherwise. Same with simple navigation, we use a combination of individual and collaborative rewards to enhance coordination.

E.3 MULTI-AGENT QUADRUPED ENVIRONMENTS

(*Realistic, limited observability, high-dimensional observation space, cooperative, and robotics*) MQE is an Isaac Gym–based simulator that marries physically accurate rigid-body dynamics with massively parallel GPU execution. Each robot, Unitree Go1, is modelled with 12–18 actuated degrees of freedom, ground–contact friction, and joint-space torque limits, enabling realistic behaviors such as trotting, bounding, and recovery from perturbations. The platform natively supports heterogeneous morphologies, randomized terrain tiles, and object manipulation, making it ideal for testing coordination and communication under high-dimensional, contact-rich dynamics. In this testbed, we consider three scenarios: Go1Gate, Go1Sheep-Hard, and Go1Seesaw.

Go1Gate: Two Unitree Go1 robots must pass through a constricted opening of width w_{gate} and reach a specified goal region on the opposite side within a horizon of T_{max} timesteps, all without colliding with the gate boundaries and another robot. Success demands precise alignment of the robot’s heading and finely tuned speed control to negotiate the narrow aperture; any contact incurs a collision penalty, while a clean, collision-free traversal earns a completion bonus. This task, therefore, emphasizes agile steering, dynamic balance, and minimal lateral deviation from the gate centerline to ensure efficient and safe passage.

For training with privileged information at each timestep, agent i has access to

$$s^i = \left[\underbrace{\mathbf{p}_i}_{6}, \underbrace{\mathbf{p}_j}_{6}, \underbrace{\mathbf{g}}_{2}, \underbrace{\mathbf{q}_i}_{4}, \underbrace{\mathbf{v}_i}_{3}, \underbrace{\boldsymbol{\omega}_i}_{3}, \underbrace{\mathbf{d}_i}_{12}, \underbrace{\dot{\mathbf{d}}_i}_{12}, \underbrace{\mathbf{a}_i^{\text{last}}}_{12} \right],$$

where $\mathbf{p}_i = [x_i, y_i, z_i, \text{roll}_i, \text{pitch}_i, \text{yaw}_i] \in \mathbb{R}^6$ is the concatenation of agent i ’s base position and orientation (Euler angles), $\mathbf{p}_j \in \mathbb{R}^6$ is the same base position and orientation of the other agent $j \neq i$ (obtained by flipping \mathbf{p}_i in the batch), $\mathbf{g} = [g_x, g_y] \in \mathbb{R}^2$ is the 2D gate position, $\mathbf{q}_i = [q_w, q_x, q_y, q_z] \in \mathbb{R}^4$ is the agent’s base orientation as a unit quaternion, $\mathbf{v}_i = [v_x, v_y, v_z] \in \mathbb{R}^3$ is the base linear velocity, $\boldsymbol{\omega}_i = [\omega_x, \omega_y, \omega_z] \in \mathbb{R}^3$ is the base angular velocity, $\mathbf{d}_i \in \mathbb{R}^{12}$ and $\dot{\mathbf{d}}_i \in \mathbb{R}^{12}$ are the per-joint positions and velocities for the 12 DoFs, and $\mathbf{a}_i^{\text{last}}$ is the previous action (torque or target position) applied at each joint.

At each timestep, agent i ’s local observation is a part of privileged information, $o_i = [\mathbf{p}_i, \mathbf{p}_j, \mathbf{g}]$. An agent i outputs an action $a_i = [v_x, v_y, \omega_{\text{yaw}}]$, where v_x, v_y are the desired linear velocities in the x, y directions and ω_{yaw} is the desired yaw rate. After performing the action, the agent i receives a reward as follows.

$$r_i^t = \underbrace{c_{\text{target}} (d_i^{t-1} - d_i^t)}_{\text{approach reward}} + \underbrace{c_{\text{col}} \mathbb{1}_{\text{col}}}_{\text{collision punishment}} + \underbrace{c_{\text{succ}} \mathbb{1}[x_i > d_{\text{gate}} + 0.25]}_{\text{Goal achievement reward}} + \underbrace{c_{\text{agent}} \frac{\mathbb{1}[d_{ij} < \delta]}{d_{ij}}}_{\text{Inter-agent distance punishment}}$$

(I) Approach reward r_i^{approach} encourages agent i to reduce its Euclidean distance to the target $d_i^t = \|[x_i^t, y_i^t] - \text{target}\|_2$. The term $d_i^{t-1} - d_i^t$ is positive when the agent moves closer, and c_{target} scales the reward magnitude. (II) Collision punishment r_i^{contact} imposes a penalty c_{col} whenever agent i collides, indicated by $\mathbb{1}_{\text{col}} = 1$. This discourages unsafe actions. (III) Goal achievement reward r_i^{success} awards a one-time bonus c_{succ} when agent i first crosses the gate threshold at $x_i > d_{\text{gate}} + 0.25$, as marked by the indicator. (IV) Inter-agent distance punishment r_i^{agent} discourages agents from crowding by penalizing when the squared inter-agent distance $d_{ij}^2 = \|[x_i, y_i] - [x_j, y_j]\|_2^2$ is below δ . The penalty $c_{\text{agent}}/d_{ij}^2$ grows as they get closer.

Go1Sheep-Hard: In this task, two Go1 robots must guide nine simulated sheep NPCs from their initial spawn area into a designated corral within a fixed horizon of T_{max} timesteps, strictly avoiding collisions. Each sheep executes randomized maneuvers and unpredictable bursts of acceleration, demanding that the robot continuously predict their future positions and adjust its steering and speed with high agility. Task success hinges on efficiently reducing the Euclidean distance between the robot and each sheep to enable timely interception, steering the flock toward the corral boundary, and preserving a safe buffer to prevent contact while the sheep actively attempt to escape capture.

For Go1Sheep MDP, privileged information first is defined as follows:

$$s^i = \left[\mathbf{p}_i, \mathbf{p}_j, \mathbf{g}, \underbrace{\mathbf{m}}_{2 \times 9}, \mathbf{q}_i, \mathbf{v}_i, \boldsymbol{\omega}_i, \mathbf{d}_i, \dot{\mathbf{d}}_i, \mathbf{a}_i^{\text{last}} \right],$$

where $\mathbf{m} = [x_{\text{npc}1}, y_{\text{npc}1}, \dots, x_{\text{npc}9}, y_{\text{npc}9}]$ are the 2D positions of the nine ‘sheep’ NPCs. The observation is $o_i = [\mathbf{p}_i, \mathbf{p}_j, \mathbf{g}, \mathbf{m}]$, and action is same with Go1Gate. The reward is defined as follows.

$$r_i^t = \underbrace{c_{\text{succ}} \sum_{m=1}^M \mathbb{1}[x_{s_m}^t > d_{\text{gate}}]}_{\text{Success shepherding reward}} + \underbrace{\begin{cases} c_{\text{mix}}, & x_{s_m}^t \geq d_{\text{gate}}, \\ c_{\text{mix}} \exp\left(-\frac{\|[x_{s_m}^t, y_{s_m}^t] - \mathbf{g}\|}{2}\right), & \text{otherwise} \end{cases}}_{\text{Mixed sheep reward}}$$

(I) Success shepherding reward r_i^{success} encourages the agent to drive all NPCs across the gate. Let $\text{cross}_{e,m} = \mathbb{1}[x_{s_{e,m}}^t > d_{\text{gate}}]$, $S = \sum_{m=1}^9 \text{cross}_m$. Then each agent in environment receives $r_i^{\text{success}} = c_{\text{succ}} S$. This one-time shaping reward is added each timestep after any sheep crosses the gate, and is reset when the environment resets. **(II)** Mixed sheep reward r_i^{mixed} provides a continuous shaping signal based on each sheep’s proximity to the gate. In this shaping scheme, we first compute the two-dimensional Euclidean distance $D = \|(x, y) - \mathbf{g}\|_2$ between each sheep’s position (x, y) and the gate center \mathbf{g} . The per-sheep reward r_{mixed} is then defined as $r_i^{\text{mixed}} = c_{\text{mix}}$ when $x \geq d_{\text{gate}}$, otherwise, $r_i^{\text{mixed}} = c_{\text{mix}} \exp(-D/2)$, so that once a sheep crosses the gate threshold d_{gate} it immediately earns the full shaping scale c_{mix} , while before crossing it receives a smoothly increasing bonus that decays exponentially with distance. Summing these per-sheep terms over all sheep produces the total mixed-sheep reward, which therefore rises continuously as the flock approaches the gate and caps at c_{mix} upon passage.

Go1Seesaw: Two Unitree Go1 quadrupeds must coordinate to exploit a lever-style plank and climb onto an adjacent elevated platform within a maximum of T_{max} timesteps, without causing the seesaw to collapse. Starting on one side of a suspended flat board, one robot must position itself at the far end to counterbalance and stabilize the seesaw’s pivot, while the second robot ascends the inclined plank to reach the platform. Precise timing of weight distribution, agile modulation of stance to damp oscillations, and real-time adaptation to shifting center-of-mass dynamics are all required to maintain balance and complete the ascent successfully.

In this task, privileged information is defined as $s^i = [\mathbf{p}_i, \mathbf{p}_j, \mathbf{q}_i, \mathbf{v}_i, \omega_i, \mathbf{d}_i, \dot{\mathbf{d}}_i, \mathbf{a}_i^{\text{last}}]$, the observation $o^i = [\mathbf{p}_i, \mathbf{p}_j]$, and action is same with other tasks. Lastly, the reward is defined as follows.

$$r_i^t = \underbrace{c_x \left(\sum_{i=1}^2 x_i^t - \sum_{i=1}^2 x_i^{t-1} \right)}_{\text{x-movement reward}} + \underbrace{c_h \left(\sum_{i=1}^2 z_i^t - 0.56N \right)}_{\text{Height reward}} + \underbrace{c_y \left(\sum_{i=1}^2 (y_i^t)^2 - 0.5N \right)}_{\text{Lateral-deviation punishment}} + c_{\text{col}} \mathbb{1}_{\text{col}}^t + \underbrace{\frac{c_{\text{dist}} \mathbb{1}[d_{ij}^t < 0.5]}{(d_{ij}^t)^2}}_{\text{Inter-agent distance punishment}} + \underbrace{c_{\text{succ}} \sum_{i=1}^2 \mathbb{1}[x_i^t > 7.7 \wedge z_i^t > 1.3]}_{\text{Goal achievement reward}} + \underbrace{c_{\text{fall}} \mathbb{1}_{\text{fall}}^t}_{\text{fallpunishment}}$$

(I) x-movement reward r^{move} encourages the robots to collectively advance along the plank by rewarding positive change in their fore-aft positions. **(II)** Height reward r^{height} incentivizes climbing by granting a bonus whenever the team’s average elevation exceeds the nominal stance height. In this term, Z -coordinates above the nominal standing height (0.56m) earn a bonus. **(III)** Lateral-deviation punishment r^y penalizes straying from the centerline by imposing a cost for large side-to-side displacements, thereby keeping the bases near the seesaw’s centerline. **(IV)** Collision punishment r^{col} discourages unsafe contacts by applying a fixed penalty whenever any robot registers an external collision, promoting safe foot placements and mutual avoidance. **(V)** Inter-agent distance punishment r^{dist} prevents crowding by sharply penalizing pairs of robots whose planar separation drops below 0.5m. **(VI)** Goal achievement reward r^{succ} rewards task completion by giving each robot a one-time bonus when it steps cleanly onto the far platform ($x > 7.7$ m and $z > 1.3$ m). **(VII)** Fall punishment r^{fall} strongly discourages loss of balance by penalizing any roll- or pitch-termination event.

E.4 BI-DEXHANDS

(*Realistic, limited observability, high-dimensional observation space, high-dimensional action space, cooperative, and robotics*) Bi-DexHands is a high-fidelity bimanual manipulation benchmark built in Isaac Gym, pairing two Shadow Hands in richly contact-driven tasks. In this work, we focus on three prototypical scenarios, *i.e.*, Door Open Outward, Bottle Cap, and Two Catch Underarm, each stressing different aspects of coordinated wrist and finger control. We select this testbed to push RL toward human-level dexterity for several reasons: Isaac Gym’s GPU parallelism delivers massive sample efficiency; the dual-hand setup embodies heterogeneous-agent cooperation in a very high-dimensional action space; and the tasks themselves are grounded in cognitive studies of fine-motor skill development, enabling evaluation of skill acquisition stages.

Door Open Outward: In this bimanual lever task, one Shadow Hand must firmly grasp a hinged door handle while the other pushes the door open away from the robot, reaching a target angle before T_{\max} timesteps, without dropping the handle or colliding with the door frame. Success demands that the “grasp” hand maintain a stable closure force as the “push” hand applies a sustained outward force and trajectory, balancing leverage and support. This challenge, therefore, stresses persistent contact stability, force distribution between hands, and dynamic coordination to overcome hinge resistance. From the viewpoint of human development, this task can be performed after 13 months (Weiss et al., 2010).

Privileged information for Door Open Outward is defined as follows:

$$s^t \in \mathbb{R}^{428} = [s^{\text{RH},t}, s^{\text{LH},t}, s^{\text{door},t}],$$

where the superscripts “RH” and “LH” denote the Right and Left Hand blocks (each of dimension 199, total 398), and “door” the 30-dimensional door/goal block.

In particular, each 199-dimensional hand block $s^{\text{H},t}$ (for $\text{H} \in \{\text{RH}, \text{LH}\}$) we further decompose as follows. Joint positions $[s_{0:23}^{\text{H},t}] \in \mathbb{R}^{24}$, Joint velocities $[s_{24:47}^{\text{H},t}] \in \mathbb{R}^{24}$, Joint efforts $[s_{48:71}^{\text{H},t}] \in \mathbb{R}^{24}$, Fingertip kinematics (positions, linear and angular velocities) $[s_{72:136}^{\text{H},t}] \in \mathbb{R}^{65}$, Fingertip forces and torques $[s_{137:166}^{\text{H},t}] \in \mathbb{R}^{30}$, Base position $[s_{167:169}^{\text{H},t}] \in \mathbb{R}^3$, Base orientation (roll, pitch, yaw) $[s_{170:172}^{\text{H},t}] \in \mathbb{R}^3$, Previous action commands $[s_{173:198}^{\text{H},t}] \in \mathbb{R}^{26}$. The remaining 30 dimensions $s^{\text{door},t}$ encode the door’s pose (7), linear velocity (3), angular velocity (3), goal pose (7), and the right/left handle positions (3 + 3), in that order.

Each hand gets its own hand and object information as a local observation at a timestep t .

Next, the action at time t is a 26-dimensional continuous vector for each hand, $a^t = [a_{0:25}^t] \in \mathbb{R}^{26}$, which we partition into six contiguous blocks:

$$a^t = \left[\underbrace{a_{0:19}^{\text{RH}}}_{\text{Hand joint commands}}, \underbrace{a_{20:22}^{\text{RH}}}_{\text{Hand base pose}}, \underbrace{a_{23:25}^{\text{RH}}}_{\text{Hand orientations}} \right].$$

In particular, $a_{0:19}^{\text{H}}$ and $a_{26:45}^{\text{LH}}$ are the 20 per-hand joint actuator targets, and $a_{20:22}^{\text{H}}$, $a_{46:48}^{\text{LH}}$ are the palm translations (x, y, z), and $a_{23:25}^{\text{H}}$, $a_{49:51}^{\text{LH}}$ are the palm orientations (roll, pitch, yaw).

At every step, the agent earns

$$r = 0.2 - \|x_{\ell\text{hand}} - x_{\ell\text{handle}}\|_2 - \|x_{r\text{hand}} - x_{r\text{handle}}\|_2 + 2 \|x_{\ell\text{handle}} - x_{r\text{handle}}\|_2.$$

The two negative terms penalize any drift from each handle, ensuring firm contact, while the final term encourages opening by increasing the handle-to-handle separation.

Open Bottle Cap: The dual Shadow Hands must grasp a bottle body and its screw-on cap, then unscrew the cap outward by applying controlled counter-rotational torque, all within T_{\max} timesteps and without slip or excessive force. One hand holds the bottle steady while the other hand applies a precise twisting motion to overcome the cap’s friction; any loss of grip or collision with the bottle incurs a penalty, whereas a clean uncapping within the time limit yields a completion bonus. This scenario highlights coordinated torque control, compliant grip modulation, and synchronized wrist rotation. From the viewpoint of human development, this task can be performed after 30 months (Zubler et al., 2022).

Privileged information for Open Bottle Cap is defined as follows:

$$s^t \in \mathbb{R}^{417} = [s^{\text{RH},t}, s^{\text{LH},t}, s^{\text{bottle},t}, s^{\text{cap},t}],$$

where $s^{\text{bottle},t}$ and $s^{\text{cap},t}$ is information related to task objects. First, $s^{\text{bottle},t}$ includes bottle pose (position and orientation quaternion; 7), linear velocity (3), and angular velocity (3). Next, $s^{\text{cap},t}$ can be decomposed as cap position (3) and cap up vector (3).

The reward combines hand-to-object proximity penalties with a strong shaping term for cap separation:

$$r = 0.2 - \|x_{\ell\text{hand}} - x_{\text{cap}}\|_2 - \|x_{r\text{hand}} - x_{\text{bottle}}\|_2 + 30 \|x_{\text{bottle}} - x_{\text{cap}}\|_2.$$

Here the first two negative terms discourage loss of contact, one hand holding the bottle body and the other gripping the cap, while the large coefficient on $\|x_{\text{bottle}} - x_{\text{cap}}\|$ sharply rewards successful unscrewing by maximizing the distance between bottle and cap.

Two Catch Underarm: Two Shadow Hands must cooperatively toss and catch two rigid objects underarm within a fixed horizon of T_{max} timesteps, without dropping either object. Success requires precisely timed wrist and finger trajectories to launch each object into free flight and intercept it in the opposite palm, while maintaining stable hand poses to avoid collision between the hands and the objects. This task, therefore, emphasizes accurate throw, catch timing, trajectory prediction, and rapid coordination of dual manipulators under gravity. From the viewpoint of human development, this task can be performed after becoming an adult.

Privileged information for Two Catch Underarm is defined as follows:

$$s^t \in \mathbb{R}^{417} = [s^{\text{RH},t}, s^{\text{LH},t}, s^{\text{object 1},t}, s^{\text{object 2},t}],$$

where $s^{\text{object},t}$ comprises of object pose (position and orientation quaternion; 7), linear velocity (3), angular velocity (3), goal pose (desired pose; 7), and rotational error between object and goal (4).

At each timestep, the agent receives a reward that sums two exponential pose-error terms, one for each object:

$$r = \exp[-0.2(\alpha d_{t1} + d_{r1})] + \exp[-0.2(\alpha d_{t2} + d_{r2})],$$

where $d_{ti} = \|x_{o_i} - x_{g_i}\|_2$ is the Euclidean distance between object i and its goal, and $d_{r_i} = 2 \arcsin(\text{clamp}(\|da_i\|_2, 1))$ measures the rotational misalignment. The dual-exponential form sharply penalizes both translational and rotational errors for each throw-catch pair, driving the hands to synchronize their toss and intercept trajectories.

E.5 HYPERPARAMETERS

Hyperparameter	Value
Max steps of an episode	1000 (MetaDrive), 50 (SN), 60 (MT), 200 (MQE), 400 (BiDexHands)
Total timesteps	10^6 (MetaDrive), 2×10^5 (Robotarium), 10^7 (MQE, BiDexHands)
The number of multi-threads	16 (MetaDrive), 32 (Robotarium), 250 (MQE and BiDexHands)
Batch size	num threads \times buffer length \times num agents
Mini batch size	batch size / mini-batch
Dimensions for communication processor	128
Dimensions for latent	32
Balancing coefficient of interactive loss	0.05
Balancing coefficient of world loss	0.05
The number of heads for communication processor	4
Commitment coefficient	0.1
Value loss	Huber loss
Threshold of Huber loss	10.0
Recurrent data chunk length	10
Dimensions for policy	[128]
Dimensions for value	[128]
Clip coefficient of PPO	0.2
Discount factor	0.99
GAE lamda	0.95
Gradient clip norm	10.0
Optimizer epsilon	10^{-5}
Weight decay	0
policy learning rate	3×10^{-4}
value learning rate	3×10^{-4}
Optimizer	Adam
RL network initialization	Orthogonal
Use reward normalization	True
Use feature normalization	True

E.6 BASELINE ALGORITHMS

This work benchmarks four MARL baseline algorithms. The implementation code adheres closely to the aforementioned official code as follows.

- MAPPO: <https://github.com/zoeyuchao/mappo>
- MAT: <https://github.com/PKU-MARL/Multi-Agent-Transformer>
- MAGIC: <https://github.com/CORE-Robotics-Lab/MAGIC>
- CommFormer: <https://github.com/charleshsc/CommFormer>

F ADDITIONAL RESULTS

F.1 ABLATION STUDY

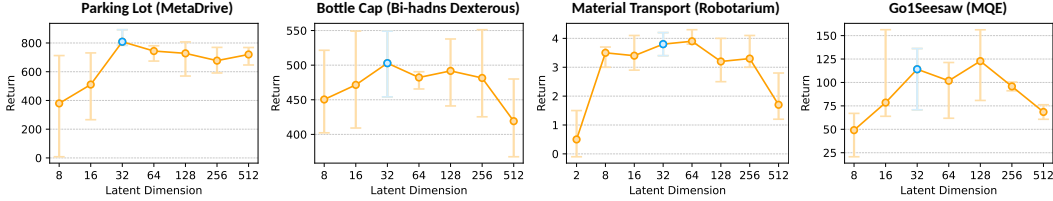


Figure 10: **Ablation study of latent dimension for MARL.** In four testbeds, $D = 32$ generally leads to the best or near-best performance.

Figure 10 plots the effect of the interactive world latent dimension $\mathcal{Z} \in \mathbb{R}^D$ on coordination performance across four diverse tasks. We evaluate $D = \{8, 16, 32, 64, 128, 256, 512\}$ and display average return with a tolerance interval. In all environments, performance rises sharply as D increases from 8 to 32, peaks or plateaus in the range $32 \leq D \leq 128$, and then degrades slightly at very high dimensions, suggesting that overly small latent spaces underfit inter-agent and world structure, while excessively large ones suffer from over-parameterization. Based on these results, we choose $D = 32$ for all main experiments.

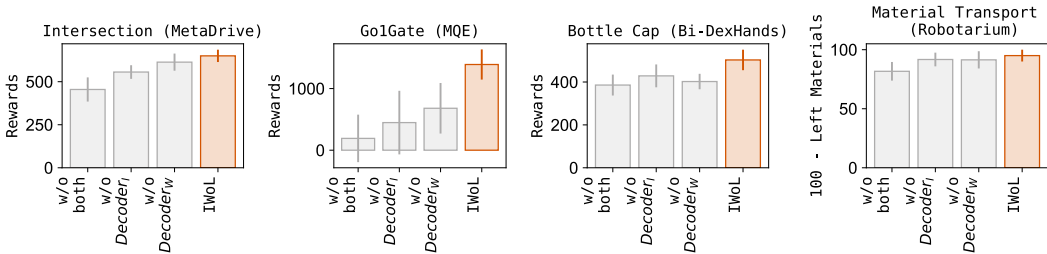


Figure 11: **Ablation study of Decoder_W and Decoder_I.** Across four challenging tasks, Decoder_W and Decoder_I are important for multi-agent coordination.

Figure 11 shows the effect of our contributed modules, Decoder_W and Decoder_I on coordination performance across four tasks. This result confirms that these modules substantially influence the performance of IWOL. More precisely, in MQE and MetaDrive, removing either decoder leads to drastic reward degradation, effectively preventing coordination. In Bi-DexHands and Robotarium scenarios, IWOL with both modules achieves the most stable and highest performance. This indicates that Decoder_W and Decoder_I play complementary roles, the former capturing world-level dynamics and the latter modeling agent interactions, together enabling robust coordination.

F.2 TRAINING TIME

To assess the practical training cost of IWOL, we report wall-clock times for all baselines across representative environments. In MetaDrive, Im-IWOL and Ex-IWOL require 8 and 10 hours, respectively, comparable to MAPPO (8h) and notably faster than MAT (11h), CommFormer (13h), and MAGIC (9h). In Bi-DexHands, where coordination and contact-rich manipulation increase complexity, Im-IWOL trains in 13 hours and Ex-IWOL in 17 hours faster than CommFormer (20h) and MAT (18h), and similar to MAGIC (15h), though MAPPO remains the fastest at 6 hours. A similar pattern emerges in Go1 Tasks, with IWOL variants showing 13 – 17 hours of training time versus 15 – 20 hours for communication-based baselines, and MAPPO again finishing in 6 hours. These results suggest that IWOL achieves strong performance with modest additional overhead compared to message-free methods, and substantially better scalability than Transformer-based communicators.

F.3 INFERENCE TIME AT DEPLOYMENT

Figure 12 compares the average inference time for each agent in four environments across all baselines. MAPPO serves as the lightweight baseline, while MAT, with its full transformer encoder, and explicit communication baselines, requiring per-step message exchanges, both incur noticeable overhead. By contrast, Im-IWoL reuses its pretrained latent encoder and adds only a small fully-connected projection on top of the MAPPO. As a result, its runtime is virtually indistinguishable from MAPPO and substantially faster than both MAT and explicit communication, demonstrating that learned representations can boost coordination without sacrificing efficiency.

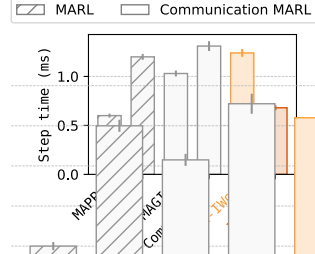


Figure 12: **Inference run time.** Wall-clock time for each agent.

F.4 COMPARISON WITH ICP

Although we claim the differences of fundamental idea between ICP and IWoL in RQ5, this subsection takes into account the following research question: **How well Im-IWoL performs compared to previous Implicit Communication Protocols in robotics frameworks?**

Implicit Channel Protocol (ICP), most recent work, enables agents to communicate without a dedicated messaging channel by treating certain observable actions as encoded signals in the environment. At each time step, an agent chooses between a scouting action $u^s = \mathcal{P}(m)$ to transmit message m via a predefined bijection $\mathcal{P}: M \rightarrow U^s$, or a regular action u^r to affect the environment. Other agents observe u^s in their next local observation and recover m by applying the inverse mapping \mathcal{P}^{-1} . Through this mechanism, ICP realizes implicit communication as inverse modeling: the behavior itself becomes the communication signal.

While (Wang et al., 2025) shows that ICP achieves better performance than other branches, these empirical results in discrete extensive-form game tasks are based on some assumptions.

- **Signal broadcast:** When an agent executes u^s , the environment inserts that action identifier into every other agent’s next observation, ensuring universal message delivery.
- **Perfect encoding/decoding:** There exists a bijective mapping $\mathcal{P}/\mathcal{P}^{-1}$ between messages M and scouting actions U^s , allowing lossless recovery.

These premises rely on perfectly and instantaneously observing every other agent’s actions, an idealization that is often violated in robotics and other real-world domains.

Consequently, we extend the ICP module to align with our experiments. First, we introduce a shared replay buffer that logs every agent’s executed actions to train the encoder and decoder. In other words, the multiple agents use a homogeneous encoder and decoder module in the execution phase to decode other agents’ embedded actions. Additionally, we maintain the signal broadcast assumption, that is, each agent can observe others’ embedded actions as a detectable environmental factor. Lastly, we adopt the three types of value functions: fully decentralized value function (ICP-Dec), global value function as the sum of individual value function (ICP-Sum), and global value function as the monotonic mixing of individual value function (ICP-Monotonic) in the training phase.

In the main text, Table 3 shows the performance comparison between Im-IWoL and ICP variants in three tasks. First of all, Im-IWoL demonstrates clear superiority compared to ICP. Both ICP-Sum and ICP-Monotonic consistently exceed the fully decentralized baseline by leveraging structured value decomposition and state-conditioned mixing to better capture inter-agent dependencies. Monotonic mixing affords further gains in tasks demanding tight coordination, while the simpler sum-of-values approach already delivers substantial robustness; in particular, it works better than ICP-Sum in the MetaDrive where multiple agents share the environment compared to other scenarios. In contrast, the fully decentralized variant struggles to scale as complexity grows. These results underscore the critical role of principled value combination in enhancing implicit communication and cooperative behavior.

F.5 IWOL WITH OFF-POLICY FAMILY ALGORITHM

In the main body, we only consider the on-policy family of algorithms. That is because they empirically provide stable and reliable training compared to the off-policy family. Additionally, all of our selected baselines are formulated as on-policy algorithms, so adhering to on-policy ensures a fair comparison and evaluation of performance.

This subsection investigates whether IWOL can be adopted within the off-policy family of algorithms.

Table 4: IWOL’s performance in off-policy algorithm.

Task	Algorithms			
	MAPPO	MAGIC	MADDPG	MADDPG+IWOL
Intersection	454.8 \pm 70.2	518.3 \pm 77.4	413.8 \pm 188.7	506.1 \pm 95.7
Parking Lot	327.4 \pm 211.7	371.2 \pm 14.3	311.0 \pm 142.6	459.3 \pm 88.2

Table 4 MADDPG+IWOL consistently improves over vanilla MADDPG, demonstrating that IWOL can also be effectively applied in off-policy settings. These results reinforce the generality and effectiveness of our communication framework, beyond the on-policy family.

F.6 FULL TRAINING CURVE

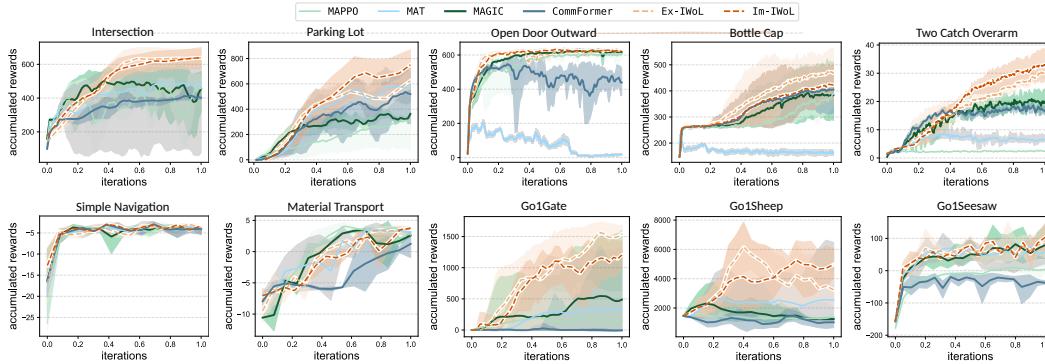


Figure 13: Learning curves across four environments. We plot the averaged rewards as a solid line and the tolerance interval as a shaded area.